Universiteit Utrecht

Institute for Theoretical Physics

Debye Institute for Nanomaterials Science

Master Thesis Theoretical Physics

Ion Transport in Tapered Nanoslits

Tim Elias Veenstra

November 21, 2022

Daily supervisors:

Dr. Gerardo Campos-Villalobos
Debye Institute for Nanomaterials Science

Dr. Giuliana Giunta
Debye Institute for Nanomaterials Science

Supervisors:

Prof. dr. ir. Marjolein Dijkstra
Debye Institute for Nanomaterials Science

Prof. dr. René van Roij
Institute for Theoretical Physics

Abstract

Over the last two decades, extensive research has been conducted in the field of nanofluidics, which focuses on the transport of water and ions in nanochannels. Recent advances have allowed the fabrication of quasi two-dimensional nanoslits, which have already been shown to exhibit many fascinating properties. In this thesis, we investigate the transport phenomena inside uncharged asymmetric, tapered nanoslits. We performed extensive molecular dynamics simulations with different geometry parameters, electric field strengths and salts, all with an explicit water model. In these systems we find a slight rectification of the ionic currents. More interestingly, we observe a strong ion selectivity, and hence a nearly diodic ion flux. We attribute this to a divergence in the polarization of the water, in combination with a high water flux. We describe the interaction between the water structure, ion fluxes and water fluxes, which acts as a novel mechanism for ion selectivity in nanoslits.

Contents

1 Introduction

All of us are familiar with salt. We regularly use it in our daily lives, for instance to season our food and prevent it from tasting horribly bland. Moreover, salts play a vital role in many biological processes that make life possible. Recounting all the different mechanisms in living organisms that rely on ions would be an impossible task. For instance, they help cells maintain osmotic pressure [1], allow muscle cells to function [2], and make brain activity possible [3]. Neurons only function due to controlled transport of ions in and out of their cells in response to certain electrical signals. It should then not come as a surprise that biological organisms have evolved a wide variety of intricate ways to transport water and ions in and out of cells. This is done by special protein complexes in their membranes that act as biological nanochannels [4].

These biological nanochannels exhibit many fascinating properties [5]. A prime example of that is aquaporin, which is an hourglass-shaped water channel protein that is ubiquitous in nature. Various types of aquaporin proteins are found in all kinds of life forms, from animals and plants to bacteria and fungi [6]. These proteins allow water molecules to be transported much more rapidly than through normal diffusion, while preventing the flow of ions, including protons. These channels are vital for the water management of cells. Another biological nanochannel that has really interesting properties is the potassium channel.[1] In many types of cells, the specific transport of potassium is very important, for instance to set the membrane potential [8]. This task is made more difficult, however, by the presence of sodium ions. Sodium and potassium ions have radii that differ by less than an ångström, and have the same electric charge. Distinguishing between the two would seem near impossible. Nevertheless, potassium channels can transport potassium without allowing any sodium to pass [9]. Vice versa, there are also channels that only transport sodium while rejecting potassium. It is thought that life could only evolve in salty ocean water thanks to these channels [10]. Ions and water in biological channels show a variety of properties that are not present in bulk systems, and so they are not just important from a biological perspective, but also from a physical perspective. In general, electrolytes that are confined in small spaces by their environment, like in ion channels, behave very differently than they would in bulk water. The interest in electrolytes goes, therefore, beyond their applications in biology. These systems are fascinating from a fundamental perspective – how the physics of electrolytes is influenced by confinement – and also because of their applications in a variety of artificial nanofluidic applications. Nanofluidics is the study of transport phenomena in systems with nanometer scale dimensions. Great strides have been made in this field that open the door for many exciting applications, some of which have the potential to have a significant societal impact.

The field of nanofluidics is relatively new, as technological challenges have prevented the fabrication of channels on the nanometer scale until very recently [11, 12]. The aforementioned biological channels provided a clue that interesting new physics could be discovered at the nanoscale, but experimental studies have long remained elusive. During the last 20 years, however, a wide variety of nanochannels has been realized, in 0D [13, 14], 1D [15–17] and 2D [18, 19]; and with a whole range of different geometries such as conical [20, 21], cylindrical [17, 22, 23] and bullet-shaped [24] channels. These efforts have yielded many new results. Fascinating phenomena were found, such as diodic [25] and transistor-like [21, 26] ion transport through conical channels, novel water phases in confinement [27], extremely low dielectric constants of water [28–30] and ion clustering [31]. Even fast water transport through carbon nanochannels was observed [15, 32–35], although it should be mentioned that the biological channels like the aquaporin still perform a bit better than the majority of the artificial ones [36]. As an aid in exploring the complex transport phenomena in nanochannels, many computational techniques are also widely used. For many systems, continuum approaches like finite-element calculations were implemented, using continuum equations like the Poisson-Nernst-Planck-Stokes equations [37–39]. We will discuss these in more detail in Section 2, but they allow a description of the system

[1] Incidentally, the discoveries of potassium channels and aquaporins were awarded a joint Nobel prize in 2003 [7].

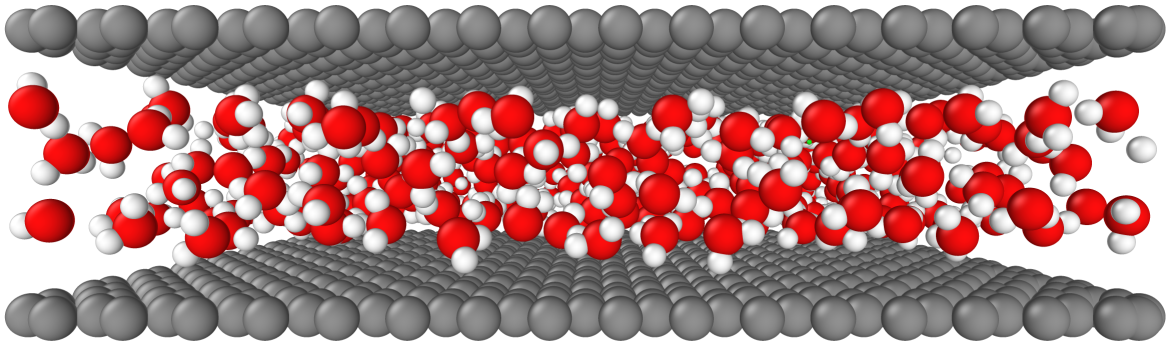

Figure 1: Quasi two-dimensional nanoslit made of graphene with a height of 1.005 nm, such that two water layers confined within. The carbon atoms that make up the graphene sheets are shown in grey, while the oxygen and hydrogen atom of the water molecules are shown in red and white, respectively.

using continuous quantities like charge densities, water velocity profiles and local fluxes. They involve bulk properties of water, such as the dielectric constant and the viscosity. When the system size is smaller and approaches the size of individual molecules and atoms, these approaches break down, however, and molecular dynamics simulations can be performed [15, 32, 33, 40–44]. Here the trajectories of all the molecules are calculated individually using Newton's laws [45]. These computational methods complement experimental studies, in that they allow for an efficient way to explore different geometries, and the dependencies on various system parameters. Constraints in computational power often limit the system size in molecular dynamics simulations, however. Nonetheless, they can help guide experimental work, and help optimizing the system parameters for various exciting applications.

Nanofluidics could help us find solutions to some of the world's biggest problems. A key example is the shortage of drinking water experienced around the globe, which is only being exacerbated by global warming and global population growth. There are more than 1.1 billion people worldwide who do not have access to safe drinking water [46]. Desalinating salt water could potentially provide a great amount of drinking water, as about 97% of water on earth is non-potable. If even a small fraction thereof could be converted into fresh water, this could have a huge impact [47]. Nanochannels embedded in membranes could play a big role in achieving this. Membranes utilizing a technology called Reverse Osmosis (RO) are much more energy efficient than presently used thermal desalination techniques and can be used on industrial scales [48]. The main challenge of these technologies is finding a trade-off between ion selectivity on the one hand, and permeability on the other [48], and knowledge on the behaviour of electrolytes in various type of channels is vital for the development of improved desalination techniques. Another exciting artificial application of nanofluidics concerns energy generation. Energy can be harvested, for instance, from mixing fresh water with sea water [17, 24, 49–52], *e.g.* where a river of fresh water meets the sea. This is a potential green energy source, which could help combat global warming. All of these applications have in common that they require a great level of control of the transport of ions and water.

In this thesis, we will focus on quasi two-dimensional channels. Major advances in material sciences in the last two decades [53, 54] have laid the foundation for the experimental fabrication of these two-dimensional graphene nanoslits in the last few years [18, 19, 41]. Nanoslits exhibit fascinating phenomena. For instance, they only allow discrete layers of water inside [55], an example of which is shown in Fig. 1 which depicts a graphene nanoslit that contains two layers of water. Graphene nanoslits that only allow a monolayer of water even turn out to completely reject all hydrated ions

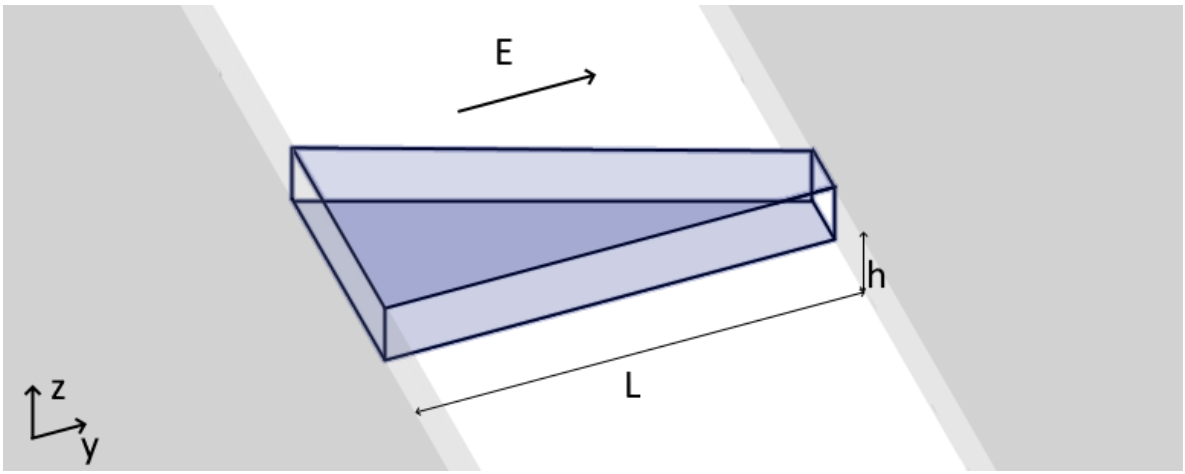

Figure 2: Three-dimensional sketch of the type of geometry that we will study in this thesis. The precise details will be elaborated on in Section 3. The electric field $\boldsymbol{E}$ point in the y direction. The channel has a constant height h and a length L.

[56], no matter their size, and similar effects have been achieved in graphene oxide nanoslits [57]. This is very exciting for desalination purposes [58, 59], as it allows water to pass through, but no ions at all. In addition to the implications for desalination technology, they have also been shown to exhibit very long-range correlations and even memory effects [60]. This would potentially allow these nanoslits to be used in neuromorphic computing. We will further discuss this in Sections 2. A lot of very intriguing physics is found in these systems, which we will try to extend in this thesis.

We will investigate these quasi two-dimensional nanoslits with molecular dynamics simulations. Specifically we try to find systems that exhibit asymmetric ionic currents or fluxes. This is an important feature of nanochannels for many of the aforementioned applications, and would add extra capabilities to the toolbox available for biomimetic and nanofluidic devices, as these properties have not yet been investigated in much detail in fully two-dimensional channels. With systems that exhibit asymmetric currents and fluxes one has control over the transport of specific ionic species. Many studies have been done on this in conical channels, as we will also see in Section 2, but not that much is known about asymmetric two-dimensional channels. We introduce this asymmetry with tapered sidewalls, such that a trapezoidal channel of length L is formed. The height h is kept constant throughout the system. A sketch of the type of two-dimensional systems that we will investigate is shown in Fig. 2. We will investigate currents and fluxes due to an in-plane electric field, without any applied pressure gradients.

In this thesis, we will first in Section 2 go over some of the relevant literature and theory on nanofluidics, previous work and recent developments in quasi two-dimensional systems. We will continue with describing our methodology in simulating these systems in Section 3. Then we will show in Section 4 that this geometry can lead not only to asymmetric currents with respect to the direction of the electric field, but also to strong ion selectivity of the channel. We attribute this to a divergence in the polarization of the water, in conjunction with a strong water flux through the channel. We then investigate these novel mechanisms and discuss their consequences and applicability.

2 Theory

As mentioned in the previous section, we will focus on a relatively new type of nanofluidics for which the continuum approaches fail. This could perhaps better be characterized as 'angstrofluidics' [61], after the ångström scale on which the relevant phenomena occur. To better understand the reasoning behind our approach, and to place the obtained result on this ångström scale into context, we must also discuss phenomena that have already been found to occur on the micro- and nanoscale. Afterwards, we will discuss the ångström scale systems that we will work with, the influence it has on the properties of water and ions, and possible applications for such systems.

2.1 Asymmetry on a Larger Scale

The behaviour of water and electrolytes inside nanochannels is quite different from that in bulk systems. Many of the differences lie in the much larger ratio between surface and volume inside the channel. Many materials have a surface charge when submerged in water, due to the surface chemistry and the high dielectric constant of bulk water. This surface charge will induce a charged area called the Electric Double Layer (EDL) inside the fluid due to the buildup of counterions and the depletion of co-ions. In bulk systems this will lead to negligible effects, but due to the relatively large surface area in nanochannels, this leads to new phenomena like current rectification [62], transistor-like behaviour [12, 26] and concentration polarization [63] when present in an asymmetric nanochannel.

2.1.1 Ionic Current Rectification

Among these phenomena, Ionic Current Rectification (ICR) has attracted a lot of attention over the years [64]. ICR is defined by an asymmetric current-voltage (I-V) relationship, creating a diode-like effect. This means that the conductance of the channel is dependent on the voltage, unlike the simple Ohmic resistor that is taught in high school physics. Wei *et al.* [65] first observed in 1997 that conical quartz pipets used for electrochemical measurements exhibited a fully linear, Ohmic, I-V relationship when the pipet diameter was large, but started to resemble a diode when either the diameter or the salt concentration was reduced. The pipet would appear to have a much higher conductivity for one direction of the electric field than for the other. A typical I-V relation that exhibits ICR is sketched in Fig. 3(a). Quartz has a surface charge when submerged in water, and therefore, has an electric double layer. ICR was attributed to the size of this EDL, where the rectification would occur when the EDLs would span the entire radius of the tip. We are talking about double layers with lengths in the order of magnitude of tens of nanometers, depending on the salt concentration. This finding sparked a lot of interest in asymmetric artificial nanochannels, as the rectification could be used to mimic the asymmetries of biological ion channels [5].

This rectifying behaviour was however not confined to quartz systems, or even to systems with tip radii close to the scale of the double layer. Conical channels were etched in PET (polyethylene terephthalate, also known for their use in soda bottles) with different charged coatings [20, 66, 67], to elucidate the influence and role of pore size and surface charge. It was shown that indeed the presence of an asymmetric electric double layer is responsible for the rectification, either by having a homogeneous double layer over an asymmetric channel – like a cone –, or by having an asymmetric surface charge [25, 68, 69]. There was also no need for overlapping double layers per se, as larger channels could also exhibit rectification [39, 70]. The requirements for ionic current rectifications are (i) a surface charge on the channel walls, with an associated EDL, and (ii) an asymmetry in the geometry, either by having an asymmetric shape such as a cone, or by having an asymmetric surface charge distribution [62].

The currently accepted model to understand ICR, is the accumulation/depletion model [71]. Most channels that exhibit ICR, also exhibit ion-selectivity due to their surface charge. Cations (positive ions) are driven away from a positive surface and anions (negative ions) are likewise repelled from

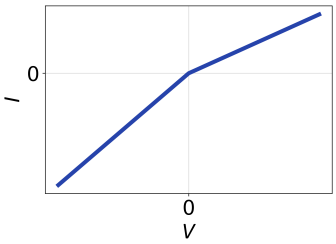

(a)

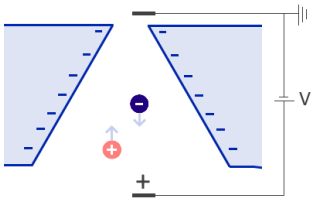

(b)

Figure 3: (a) Illustration of a current-voltage (I-V) diagram that exhibits ionic current rectification. Here the channel has a higher conductivity for negative electric fields. (b) Sketch of a conical channel with a negative surface charge, in which current rectification will occur.

negative surfaces. To illustrate this mechanism, let us consider a conical nanochannel with a negative surface charge, as shown in Fig. 3(b). When we apply a positive electric field by inserting a cathode near the wide end of the cone and grounding the reservoir near the small end of the cone, the anions will feel a 'downward' force. The channel is ion-selective due to the negative surface charge, and will repel the anions, not allowing them to enter the cone from the reservoir above the tip. This will result in a lower ion concentration at the tip, and thus a lower conductivity. Likewise, when the electric field is reversed, the anions will move 'upwards' but will be rejected by the negative charge on the walls, accumulating near the tip, and therefore increasing the conductivity. This mechanism was later confirmed by so-called Poisson-Nernst-Planck-Stokes (PNPS) calculations [37, 39], which use the Poisson, Nernst-Planck and Stokes equations. These equations describe electrostatics, ion fluxes and fluid flow, respectively, and will be discussed now.

2.1.2 The Poisson-Nernst-Planck-Stokes Equations

The Poisson-Nernst-Planck-Stokes framework is a well-known and widely used set of equations that can be used to describe electrolyte transport through nanochannels [11]. To better understand this framework, we will break it down into its different components, starting with the Poisson equation, which describes the electrostatics of the system. It is given by

$$\nabla^2 \Psi(\boldsymbol{r}) = -\frac{e}{\varepsilon}\rho_e(\boldsymbol{r}), \tag{2.1}$$

where $\Psi(\boldsymbol{r})$ is the local electrostatic potential, e is the elementary charge, ε is the dielectric constant, and $\rho_e(\boldsymbol{r})$ is the distribution of charges in the system. Eq. (2.1) relates the electric potential to the charges that are present. These charges can have the form of surface charges, or of a net ionic charge $\rho_e(\boldsymbol{r}) = q_+\rho_+(\boldsymbol{r}) + q_-\rho_-(\boldsymbol{r})$, which is the sum of all the local ionic charges. Here, $q_\pm$ is the valency of the positive or negative ions, with $q_+ > 0$ and $q_- < 0$. This equation assumes that the system can be described at a scale that is large enough such that spatially continuous ion concentrations can reasonably be defined.

The Stokes equation describes the dynamics of the fluid[2]. For an electrolyte in steady state, it is given by

$$\eta\nabla^2\mathbf{u}(\boldsymbol{r}) = \nabla P(\boldsymbol{r}) + e\rho_e(\boldsymbol{r})\nabla\Psi(\boldsymbol{r}), \qquad \nabla\cdot\mathbf{u} = 0, \tag{2.2}$$

[2]This is a special case of the Navier-Stokes equations under the assumption that the Reynolds number $\mathrm{Re} = \rho u L/\eta$ is much smaller than 1, where ρ is the mass density of the fluid, $\boldsymbol{u}$ is a typical fluid velocity, L is a typical length scale and η is the dynamic viscosity.

where η is the dynamic viscosity, $\mathbf{u}(\boldsymbol{r})$ is the velocity of the fluid and $P(\boldsymbol{r})$ is the pressure in the system. We see that there needs to be either a pressure gradient, or a spatial charge distribution in combination with an electric field to generate a net fluid flow (assuming there is friction with surfaces, otherwise a finite constant flow profile would also be a solution, but this is unphysical in these systems). This equation again assumes that all relevant quantities such as the fluid velocity and the charge distribution to be spatially continuous and smooth.

Lastly, we have the Nernst-Planck equations, which describe the transport of ions due to diffusion, conduction and advection. It is given by

$$\mathbf{j}_{\pm}(\boldsymbol{r}) = -D_{\pm}\left(\nabla\rho_{\pm}(\boldsymbol{r}) + q_{\pm}\rho_{\pm}(\boldsymbol{r})\frac{e\nabla\Psi(\boldsymbol{r})}{kT}\right) + \mathbf{u}(\boldsymbol{r})\rho_{\pm}(\boldsymbol{r}), \tag{2.3}$$

where $\mathbf{j}_{\pm}$ is the ion flux for the positive and negative ions, respectively, $D_{\pm}$ their diffusion constants, k the Boltzmann constant, and T the temperature.

Although the PNPS equations in these forms have been used to describe electrolyte transport in 2D systems with a channel height of 1 nm [72], this set of equations breaks down for these small length scales. When considering channels with a spatial dimension of a single nanometer – as we do in this thesis – bulk values of quantities such as the dielectric constant, viscosity and diffusion constants cannot be used. The Stokes equation, and continuum hydrodynamics in general, also break down when the characteristic length scales are under 1 nm [11, 73].

The systems described in Section 2.1.1 were relatively large compared to the two-dimensional systems that we will study. The original pipets of Wei *et al.* had tip radii of roughly $20 - 40$ nm [65]. The cones that were etched in PET by Siwy *et al.* were of the order of 10 nm [20]. These length scales are small enough that they warrant a different approach from macroscopic conical pipes and that their behaviour is dominated by its charged surface. However, it is large enough that continuum theories can be used and water could be seen as a simple fluid with a dielectric constant of 80. The Poisson-Nernst-Planck-Stokes equations are still applicable here which describe continuous quantities such as salt concentrations. They are however not as small as a lot of biological channels, which have typical length scales of ångströms. At the scale of ångströms, these methods stop working, as the size of the channel starts to approach the sizes of the ions and the water molecules themselves. When we wish to investigate if similar phenomena can occur at smaller length scales, different approaches are required. Not in the least, we must think about how such a channel could be created experimentally.

2.2 The Graphene Revolution

Creating smooth two-dimensional channels requires the use of two-dimensional materials. However, purely two-dimensional materials have long been elusive. This changed with the discovery of graphene [53], for which Konstantin Novoselov and Andre Geim would later win the Nobel prize. They managed to obtain two-dimensional sheets of graphene by applying scotch tape to a piece of graphite and later dissolving the said tape. The resulting material turned out to have exceptional properties like metallicity and incredible strength [74]. Later, more two-dimensional materials were found such as hexagonal boron nitride (hBN) and molybdenum disulfide (MoS_2) [75]. It has been shown that quantum mechanical interactions between graphene and water can in some circumstances actually be significant [76], but that is well outside the scope of this thesis. We will also not discuss all the interesting electric and mechanical properties of these materials here, but focus solely on the use of graphene in the construction of new structures that can be used to make two-dimensional nanoslits.

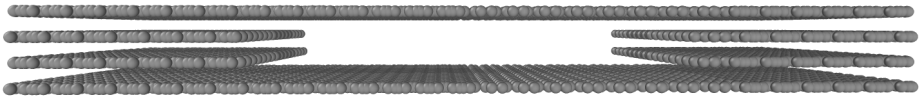

Figure 4: Illustration of a graphene nanoslit. Two sheets of graphene function as a top and bottom layer of the slit, while there are two spacer layers on either side of the slit to support them. The layer spacing is 0.335 nm, so this results in a quasi two-dimensional nanoslit with a height of 1.005 nm [75]. Figure inspired by Fig. 1a of Ref. [77].

These two-dimensional materials can be stacked together using so-called van der Waals assembly [54]. If, in this process, one or more layers are left out, as is shown in Fig. 4, an atomically flat two-dimensional slit appears which can be used as a nanochannel [77, 78]. The spacer layers between the top and bottom sheets that hold open the slit can be of the same material as the top and bottom, but can be replaced by other two-dimensional materials to influence the slit height. The chemistry of these nanoslits is also very different from that of most other nanochannels. Walls made up of glass or polymers like PET usually contain charged surface groups (also depending on the pH), while graphene can be free of such surface charge. Contaminating hydrocarbons can form in between the layers of graphene, but they tend to quickly diffuse over micrometer distances and aggregate into pockets, leaving large stretches of usable 'clean' graphene [79]. These uncharged nanoslits are a completely different environment from the charged nanochannels mentioned before. Not only will these slits be much smaller than any electric double layer would be, there is no surface charge at all that can influence the behaviour of ions in the channel. Consequently, any effects are purely geometrical.

2.3 Electrostatics in Confined Water

Even without surface charges, nanochannels exhibit many interesting properties. For instance, recent experimental work shows that the water inside a nanoslit turns out to have a very low and anisotropic dielectric constant [29]. The dielectric constant is usually a material property that is independent of shape or environment of the material, but in confinement the relative dielectric constant perpendicular to the surface can drop from its bulk value $\epsilon_b \approx 80$ down to $\epsilon_\perp \approx 2$. This is usually explained by the restriction of the orientation of water molecules near the surface [30, 80–83]; the dipoles of the water molecules near the surface cannot fully reorient themselves to align with external electric fields, effectively lowering the dielectric constant. The total dielectric constant of the confined water can then be estimated by taking an average over the 'dead' layers of water near the surface, and the 'free' layers in between. There is, however, some debate about whether the water layers near the surface are sufficiently rigid to explain the very dramatic drop in dielectric constant that was observed [84]. A new study proposed that this effect must be caused by a different mechanism altogether [85]. Olivieri *et al.* propose that the strong dipole-dipole correlation in water, that extends for nanometers, in combination with the materials of the wall that generally have a very low dielectric constant, are the cause for the decrease in the local dielectric constant near surfaces. The wall then acts effectively as an excluded volume for the dipole interactions. Numerical calculations of dielectric constants in nanoslits are difficult to converge [85], however, and more research will be needed to settle this debate.

No matter the origins of this effect, the decrease in dielectric constant inside confined channels has a dramatic influence on the behaviour of ions in such a system. Salt usually dissolves when added to bulk water because the dielectric constant in water is sufficiently high. The high dielectric constant of water, compared to that of a medium such as air, reduces the energy that is required to pull a cation and an anion apart that are held together via Coulombic attraction. The thermal energy of these ions in water is therefore enough to let the ions dissociate. This is not necessarily the case in these confined slits. In two-dimensional nanoslits ions can even cluster back together from a dissolved salt into a

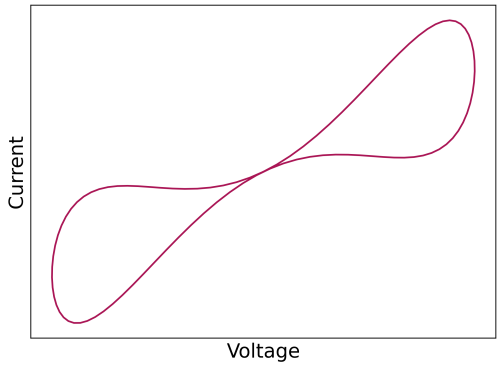

(a)

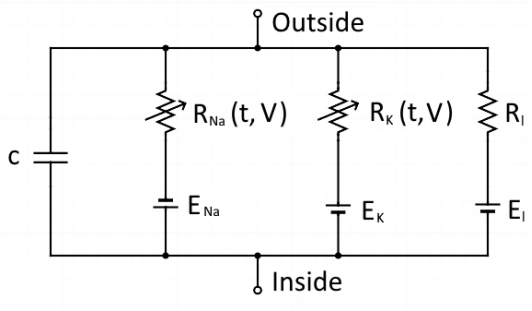

(b)

Figure 5: (a) Schematic representation of a current-voltage curve of a memristor. (b) Circuit that represents the neuron membrane in the Hodgkin-Huxley model. Based on Fig. 1 from Ref. [3]

crystal-like structure [31]. This does not only impact the number of dissolved ions in the system, but consequently also the number of ions that can contribute to currents.

2.4 The Ions Remember

Interestingly enough, the aforementioned clustering behaviour of ions does not only influence the steady state conductivity of a system but can also introduce memory effects. Robin *et al.* [60] found that there is a time scale associated with the clustering and disassembling of divalent ions when electric fields are switched on or off. When an oscillating electric field is applied with a frequency that is sufficiently high such that the system is not allowed to reach steady state, then the current can exhibit significant hysteresis. The conductivity at any given time depends on the number of free ions, which in turn depends on the electric field at earlier times.

These memory effects, are not unique to nanoslits or even ionic systems. Memristors (as these systems are often called) were proposed as a mathematical concept that was missing from circuit theory in 1971 [86]. It is defined as a relationship between electric flux and charge, but in practice it can lead to a frequency dependent 'butterfly'-like curve in the current-voltage diagram, as is sketched in Fig. 5(a) [87]. The circuit element that realized this effect remained elusive until a solid-state memristor was realized in 2008 [88]. Independently of the developments around memristors, the concept of a time-dependent resistor has been used elsewhere. In 1952, Hodgkin and Huxley published about the mathematical modelling of neurons [3]. Their work was based on experiments on the giant axon of the squid, which has the benefit of being sufficiently giant to be probed with the electrodes that were available in the 1950s.[3] They could model the neuron, and its ionic channels, with a set of differential equations. Interestingly, this model can also be realized by an electric circuit with two resistors that depend on time and the applied electric field, see Fig 5(b). In a biological cell these resistors correspond to sodium and potassium channels, which together create the voltage spike [3]. This framework accurately describes neuron activation and neuron spiking, and was a big step forward in understanding the inner working of neurons, for which they won the Nobel prize in 1963.

[3]It should be noted that 'giant squid axon' refers to the giant axon of a squid, and not an axon of a giant squid (Architeuthis dux) which is a specific species of squids. The latter is often reported, while Hodgkin and Huxley actually worked with the longfin inshore squid (Doryteuthis pealeii) [89]. On another completely irrelevant side-note: the nerves of the same species have previously been connected to an iPod, allowing researchers to control the chromatophores (which dynamically control the squid's color for camouflage) with music [90].

Based on this Hodgkin-Huxley model, Robin *et al.* showed that the memory effects of the current in the roughly two-dimensional nanoslits, can most likely be used to realize a physical version of the circuit in Fig. 5(b). They showed that this yields voltage spiking, which resembles elementary neuromorphic behaviour. This is very exciting as it allows for the design of more complex nanofluidic devices that mimic neuron activity, potentially opening the door for a host of biomimetic applications and neuromorphic computations [91, 92].

2.5 Ion Hydration in Confinement

Ions, by their very definition, carry an electric charge. Water is a polar molecule and will therefore align itself with either the slightly negative oxygen atom or one of its slightly positive hydrogen atoms towards the ion [93]. Water molecules will form a spherical shell around an ion, as sketched in Fig. 6, the diameter of which is dependent on various properties of the ion. Water molecules in the hydration shell around cations point their oxygen atom towards the ion, while water molecules near an anion point one of their hydrogen atoms towards the ion. Divalent and trivalent ions can even have two of such hydration shells, as their electric field is stronger and thus spreads farther outwards [94]. The structure of water does not only influence the dielectric constant and, consequently, the Coulomb interactions as we saw in the previous subsections, but can also directly impact the behaviour of ions via these hydration layers.

In confinement, it is not trivial that such shells exist at all times, as the small spaces in which ions can sometimes find themselves may not accommodate such extensive hydration shells. It is possible for the ions to shed some of the surrounding water when the geometry in which they are situated is not big enough for the entire shell, albeit at an energy cost [19, 95]. The structure of the new hydrating layers is dependent on both the scale and geometry of the environment [96]. Ions are not rejected from slits and channels that are slightly smaller than their hydrated radius, rather they can deform the shells to 'squeeze' into the channel. This can result in ion selectivity, since the free-energy penalty for entering a slit may be different for different ions. Moreover, when the ions have already entered the slit, their mobility is dependent on the interaction between their hydrated water molecules and the confining surfaces [19]. Water molecules near a surface such as graphene or hBN also have a preferred orientation, as their hydrogen atoms tend to point towards the surface [97]. However, near an anion they will point towards the ion, away from the surface, causing a stronger interaction between the ion and the surface. In practice this means that an anion has a lower mobility than a cation of the same size in two-dimensional confinement [42].

Ion selectivity alone will not result in any effects resembling ICR in these nanoslits. For that we will also need to add asymmetry in the geometry of the nanochannel. To the best of our knowledge,

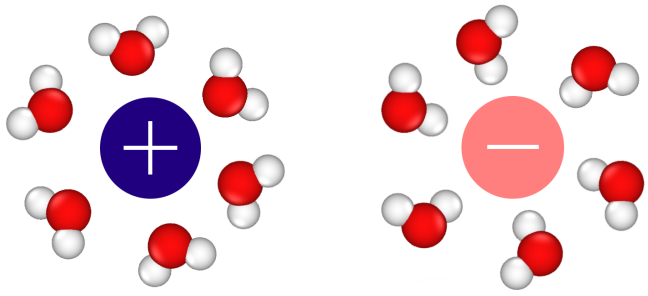

(a) (b)

Figure 6: Sketch of the hydration shells of both (a) a positive and (b) a negative ion.

there are three very recent studies that investigate similar systems [43, 44, 72]. Li *et al.* , in Refs. [43, 44] performed molecular dynamics simulations with a slightly different geometry from the one that we will investigate (which will further be discussed in Section 3). They created a graphene slit with a strongly converging slit height, through which they drove ions and observed ion selectivity. This could have important applications for filtration purposes. They propose that their asymmetric fluxes are due to asymmetric dehydration of the ions in the tip of the channel, depending on the direction of the ion flux. The disadvantage of their geometry, however, is that it is currently not possible to experimentally realize it with Van der Waals assembly, which is the state of the art method to create slits for nanofluidic purposes, while the geometry that we propose here could potentially be made. Another recent study looked experimentally at asymmetric two-dimensional graphene-oxide channels [72], with a shape very similar to the one that we will study. In contact with water, graphene oxide is a charged material, however, resulting in a system where charge-related phenomena dominate the currents. Even though their slit height is about 1 nm, their channel width and length span several millimeters, allowing them to use continuum PNPS equations to explain their experimental findings. These studies show that asymmetry is possible in systems related to the one we will study. The mechanisms that cause the asymmetries in these papers, however, are not applicable to our system as we will not consider charged surfaces, and the channel widths will be much larger than that of Li *et al.* [43, 44].

In this thesis we will study the behaviour of water and of ions in asymmetric two-dimensional nanoslits. Inspired by ICR phenomena in charged conical nanochannels, we will try to achieve ion selectivity and diodic currents with channels without any surface charge, purely by the design of their geometry. We will systematically analyze the behaviour of the water structure in our systems, the hydration of ions and the dynamics of ions and water molecules. The novelty of this thesis lies on the one hand in the geometry, which has not been studied before in literature, and on the other hand in the unique interaction between ions and water that we observe therein.

3 Modelling Electrolytes in Two-Dimensional Channels

To investigate electrolyte fluxes and currents in asymmetric nanoslits, we will perform computer simulations of electrolytes in these confined systems. In this section we outline the technical details of the simulated system and the methods of simulation.

3.1 Simulating Atoms

At the basis of our work is the explicit simulation of atoms. Since we are not dealing with ideal gases, we must take the interactions between atoms into account and calculate the forces between them. The basic interaction between two atoms can be divided into a repulsive part and an attractive part. At very short distances, mere ångströms apart, the electron orbitals of the atoms start to overlap, which is forbidden by the Pauli principle. Therefore, a sharp repulsion, chosen to be proportional to $1/r^{12}$, is added to our potential. The attractive part is caused by the Van der Waals forces, which are proportional to $1/r^6$ [98]. Combining this, we get the Lennard-Jones potential

$$\Phi_{LJ}(r_{ij}) = 4\varepsilon \left[\left(\frac{\sigma}{r_{ij}} \right)^{12} - \left(\frac{\sigma}{r_{ij}} \right)^{6} \right]. \tag{3.1}$$

Here ε is the potential well depth of the attractive part, σ is a measure of atom size and r_{ij} is the distance between particle i and j. This potential is of course an approximation, but one that works remarkably well and is a popular choice in computer simulations [45]. The parameters σ and ε are different for all atoms, so care must be taken when interactions between different elements are calculated. We use so-called geometric mixing rules, meaning that we calculate the effective Lennard-Jones parameters of two atoms with different species i and j as $\sigma = \sqrt{\sigma_i \sigma_j}$ and $\varepsilon = \sqrt{\varepsilon_i \varepsilon_j}$. The Lennard-Jones parameters that we use for each element can be found in Appendix A. Charged atoms also interact via the Coulomb potential:

$$\Phi_C(r_{ij}) = \frac{1}{4\pi\varepsilon_0\varepsilon_r} \frac{q_j}{r_{ij}}. \tag{3.2}$$

where ε_0 is the dielectric constant of vacuum, ε_r is the relative dielectric constant of the medium, and q_j is the charge of particle j. To simulate our system, we will use molecular dynamics (MD) simulations. These are implemented in the Large-scale Atomic/Molecular Massively Parallel Simulator (LAMMPS) [99]. This makes use of the well-known velocity Verlet algorithm to update the positions of all the particles each time step. The positions of particle i are updated according to

$$\mathbf{x}_i(t + \Delta t) = \mathbf{x}_i(t) + \mathbf{v}_i(t)\Delta t + \frac{1}{2}\mathbf{a}_i(t)\Delta t^2, \tag{3.3}$$

where $\mathbf{x}_i(t)$ is the position of particle i at time t, and similarly $\mathbf{v}_i(t)$ is its velocity and $\mathbf{a}_i(t)$ its acceleration. The time step Δt of the simulation is chosen to be 1 fs. The acceleration $\mathbf{a}_i(t + \Delta t)$ is then calculated at the new position with Newton's laws, after which the new velocity is calculated with:

$$\mathbf{v}_i(t + \Delta) = \mathbf{v}_i(t) + \frac{\mathbf{a}_i(t) + \mathbf{a}_i(t + \Delta t)}{2}\Delta t. \tag{3.4}$$

We use a Nose-Hoover thermostat with a damping time of 100 femtoseconds to maintain a temperature of 300 K in our system. We use a cutoff of 1 nm for the Lennard-Jones and Coulomb interactions. The long-range interactions are calculated with the Particle-Particle Particle Mesh (PPPM) method with a slab correction.

3.2 System Geometry and Surfaces

As mentioned before, we want to study very thin nanoslits, created by removing two-dimensional layers out of a layered material such as graphite [54]. This cavity is supported by spacer layers, which are usually straight. We will compare two different systems; a system where the spacer walls are straight and assumed to be infinitely far way, and a system with spacer side walls, that confine the area laterally. In the former case, we do not bother to simulate the side walls explicitly, but rather treat the channel as being infinitely wide and long by imposing periodic boundary conditions. This geometry is shown in Fig. 8. Our actual system dimensions will be 20×20 nm^2, unless stated otherwise. The height of the channel is 1.005 nm. This is the height that is obtained by removing two graphene layers from graphite, as the inter-layer spacing is 0.335 nm [75]. We will compare this nanoslit with geometries in which an asymmetry has been introduced via the spacer layers. Instead of ignoring the spacer layers, we will simulate them explicitly here, and put the spacers under an angle such that the channels are tapered. A sketch of this geometry is shown in Fig. 7. We describe the nanochannels with three parameters: D_m the average width of the channel, L the length of the channel, and $\xi = D_t/D_b$ which is the ratio between the widths D_t and D_b of the tip and base of the channel, respectively. Thus $\xi = 1$ means that the spacers are parallel to each other, while $\xi = 0$ means that the small end of the channel is completely closed. The reservoirs outside the tapered channel are also two-dimensional and, therefore, also have a height of 1.005 nm. Throughout this thesis we will always use $L = 8$ nm, and the entire system is 15×20 nm, unless stated otherwise. The origin of our coordinate system is situated in the center of the system.
From the parameters ξ, D_m, L, we can calculate all other geometry parameters. The angle α that the tapered walls make with the y-axis, is given by

$$\alpha = \arctan\left(\left(\frac{1-\xi}{1+\xi}\right)\frac{D_m}{L}\right), \tag{3.5}$$

while the width of the top D_t and bottom D_b are given by

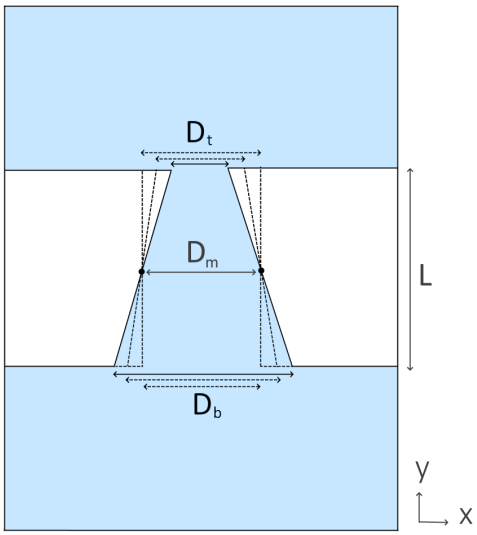

Figure 7: Tapered channel geometry with explicitly simulated spacer walls (white). Here L is the length of the channel. D_m, D_t and D_b are the width at the middle, tip and base, respectively. The tip-to-base ratio $\xi = D_t/D_b$ is varied between $\xi = 0.25$ and $\xi = 1$ as shown with the dotted lines, with a fixed value of D_m.

$$D_t = \frac{2\xi}{1+\xi} D_m; \qquad D_b = \frac{2}{1+\xi} D_m. \tag{3.6}$$

We will stick to relatively large D_m. As discussed in Section 2, Li *et al.* [43, 44] have investigated a system where the minimal height was small enough to require ions to shed their hydration shell. Although our system is different – we vary the width of the channel rather than the height – we choose to look into a different regime, where ions can fit through the channel without dehydration. We are therefore looking for other mechanisms and phenomena that have not yet been reported in the literature. Therefore we will mostly use $D_m = 60$ Å and $D_m = 40$ Å.

We can simulate the graphite layers of the top and bottom walls, as well as the spacer layer, explicitly by simulating carbon atoms, placed into a hexagonal pattern to form the graphene sheets, as shown in Fig. 8(b). This will require the computation of many interactions between atoms in the electrolyte inside the channel, and the constituent atoms of the walls. It would be more efficient if we could find an accurate wall potential, with which we could calculate the interaction between an atom and the wall directly from the distance between them. Considering that we simulate the carbon atoms using a Lennard-Jones potential, a popular choice for smooth wall potentials is the 9-3 LJ potential. This can be obtained by integrating out regular Lennard-Jones potentials of the carbon atoms, and assuming the walls have a uniform density. One loses the hexagonal structure of the wall, but gains a lot of computational efficiency. We consider infinitely many layers of graphene at either sides of the channel and use cylindrical coordinates, where x denotes the closest distance between a particle and the plane of the wall, and r and θ are the radial coordinates of this plane. The integration is performed over an infinite range:

$$\Phi(x') = \int_{-\infty}^{-x'} dx \int_0^{2\pi} d\theta \int_0^{\infty} dr 4\epsilon\rho r \left(\frac{\sigma^{12}}{(r^2+x^2)^6} - \frac{\sigma^6}{(r^2+x^2)^3} \right), \tag{3.7}$$

which results in the following wall potential as experienced by a particle at a distance x from the wall:

$$\Phi(x) = \frac{2\pi}{3} \epsilon\rho\sigma^3 \left(\frac{2\sigma^9}{15x^9} - \frac{\sigma^3}{x^3} \right) \tag{3.8}$$

where ρ is the average three-dimensional number density of carbon atoms in graphite, x is the shortest distance between the surface and the center of mass of the particle, and ε and σ are the Lennard-Jones parameters as discussed previously. These parameters can also be found in Appendix A

3.3 Modelling Water Molecules

Water plays an important role in the mechanisms that we are investigating. It drastically lowers the dielectric constant in the confined environment that we are simulating [29]. There are various parameterizations and models to simulate water. In this thesis we will use a particular model called SPC/E, or the Extended Single Point Charge model [101]. In this model, the H_2O atoms have a fixed internal angle of 109.4^o and a fixed bond length of 0.9572 Å. This model is often used in nanofluidic simulation studies [42, 44, 102]. Other models exist, such as the Transferable Intermolecular Potentials, TIP3P and TIP4P/2005. However, it has been shown that the TIP3P model overestimates water and ion fluxes [103]. While the TIP4P/2005 model does handle long-range interactions slightly more accurately than SPC/E [104], it is more computationally costly due to a fourth site in the water molecules that needs to be simulated. The SPC/E models also accurately predicts the diffusion constant [102] and dielectric properties [28] of bulk water, which will turn out to be important for our study. Considering all of this, we choose to use the SPC/E model. We use the SHAKE algorithm to keep the bond lengths and angles constant throughout the simulation [105].

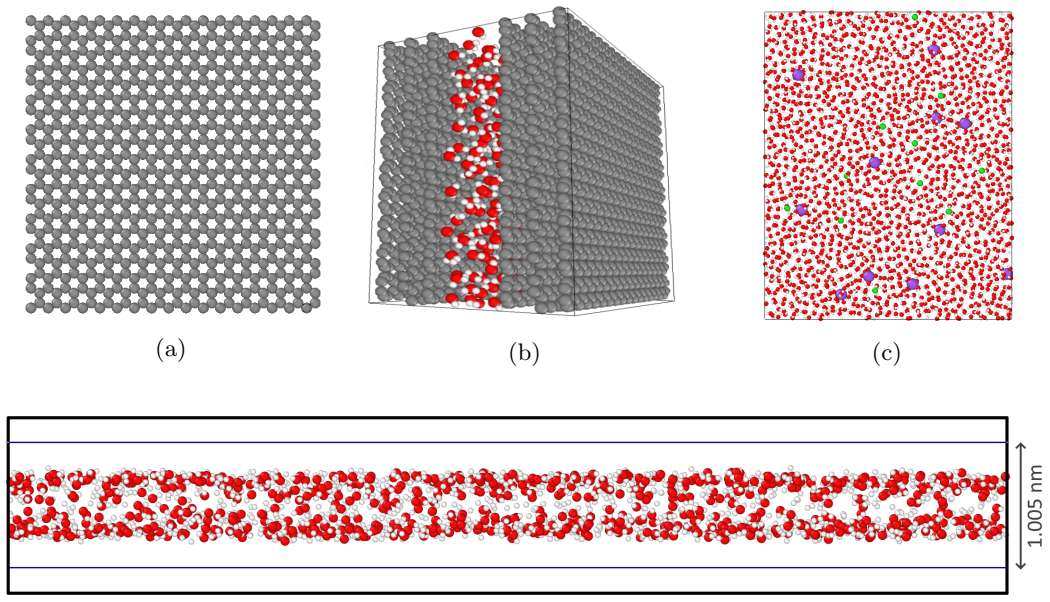

Figure 8: (a) Slab of graphene, the coordinates of which were generated with molecular visualization software VMD [100]. (b) Graphite nanoslit with inter-layer spacing of the constituent graphene slabs of 3.35 Å. The grey atoms are carbon, and the red and white atoms are oxygen and hydrogen, respectively, that form water molecules. (c) Top view of an electrolyte (Na^+ and Cl^- in purple and green, respectively) in a nanoslit confined by a Lennard-Jones 9-3 wall potential. (d) Side view of the Lennard-Jones 9-3 nanoslit (without salt). The wall is shown as a blue line. Two distinct water layers are visible.

Early preliminary calculations were done with a water area density of 0.232 $Å^{-2}$. This was the water density that was found to correspond to a slit height of 1 nm by Ref. [55]. They, however, simulate a system with graphene walls, and when we used this water concentration, we observed 'gas' bubbles appearing in our system. It is very likely that our smooth-wall approximation results in a slightly different water density compared to their system.

3.4 Grand-Canonical Monte Carlo Simulation

We need to perform so-called Grand-canonical Monte Carlo simulations (GCMC) to obtain the correct water densities. In a GCMC simulation, the chemical potential μ of the water, the system's volume V, and the temperature are kept fixed, as the system is in equilibrium with a reservoir with which it can exchange both heat and particles. In order to keep the chemical potential fixed, we have to insert and delete particles according to an acceptance rule that is determined by the imposed chemical potential μ and the energies of the system before ($E(N)$) and after the insert or deletion ($E(N \pm 1)$). Here N is the number of particles in the system. The probability of acceptance of an insertion is given by [45]:

$$\mathrm{acc}(N \to N+1) = \min\left(1, \frac{V}{(N+1)\Lambda^3} \exp\left[\beta(\mu - E(N+1) + E(N)\right]\right), \tag{3.9}$$

and the probability of accepting the removal of a particle is given by

$$\mathrm{acc}(N \to N-1) = \min\left(1, \frac{N\Lambda^3}{V} \exp\left[-\beta(\mu + E(N-1) - E(N))\right]\right), \tag{3.10}$$

where $\min(a, b)$ is the minimum of the two values, $\beta = 1/kT$, k is the Boltzmann constant, T the temperature, and Λ the thermal wavelength. We use the GCMC algorithm to keep the chemical potential of water fixed, and employ a molecular dynamics algorithm to determine the dynamics, *i.e.* rotations and displacements, of the water the molecules. Every 100 time steps, we will try to perform 100 insertions or deletions, for a total of 10^7 time steps. The average of the last $4 \cdot 10^6$ time steps will be taken as the density for this system. We perform a GCMC simulation without any salt, and with water at a chemical potential of $\mu = -10.4$ kcal/mol, which was found to be the chemical potential for bulk water at a temperature of 298 K [106]. It has been shown with GCMC simulations that this chemical potential yields a water density of $\rho = 0.23$ $Å^{-2}$ in graphene nanoslits with a height of 1.005 nm [107], which was also independently found by Ref. [55]. Performing GCMC simulations with this chemical potential in our system with Lennard-Jones 9-3 walls gives us a water density of $\rho = 0.245$ $Å^{-2}$. See Section 4 for more details on the results of the GCMC calculations.

3.5 Modeling Ions

We are interested in ionic currents and fluxes through our systems, so we have to add salt. We treat the ions canonically, *i.e.* we fix the number of ions in the system. In this thesis, we will use a salt concentration of $\rho = 7 \cdot 10^{-4}$ $Å^{-2}$. There are a lot of possible salts of course, but we will mostly focus on the monovalent salt sodium chloride (NaCl, known as table salt) and the divalent calcium sulfate ($CaSO_4$). The first one is an obvious choice, being a very common salt that is used in many studies [96]. Calcium sulfate was chosen because it is divalent, and Robin *et al.* showed that divalent salts such as calcium sulfate show interesting clustering and memory effects. Therefore, we would like to compare the monovalent salt to divalent salts in this study. If we find asymmetry in the ion fluxes in our asymmetrical channels, it would be very interesting to see if this is also present for divalent ions because this could then have applications in neuromorphic computing. We will also show results for $CaCl_2$, which will provide an interesting comparison between the two salts since it has the same cation as $CaSO_4$ and the same anion as NaCl.

As we already mentioned in Section 3.1, we model the ions as Lennard-Jones particles, of which the parameters can be found in Appendix A. The sulfate ion (SO_4^{2-}) is a molecule, however, and has a tetrahedral structure, so the oxygen atoms form angles of 109.4^o. The bond length between the sulphur atom and the oxygen atoms is 1.49Å. Each oxygen atom is assigned a charge of -1, and the sulphur atom has $+2$, yielding a total charge of -2 in electron charge units [108]. Calcium atoms have a charge of $+2$ in electron charge units. To investigate the influence of the specific LJ parameters, we will also simulate an artificial salt $X^{2+}Y^{2-}$ where X^{2+} and Y^{2-} differ only in the sign of their charge, having LJ parameters and masses identical to those of calcium. All the parameters for these ions can also be found in Appendix A. We can now apply an in-plane electric field through the slit. The walls are defined to be in the x-y plane, and the external electric field is pointed in the y-direction. The x and y directions have periodic boundary conditions. When salt is present, there will be an ion current due to the electric field. We measure the current using

$$I = \frac{e}{L_y} \left\langle \sum_i q_i \frac{y_i(t+\delta t) - y_i(t)}{\delta t} \right\rangle_t , \tag{3.11}$$

where e is the elementary charge, L_y the length of the simulation box in the y-direction, q_i is the valency of ion i, δt is the time interval and $\langle ... \rangle_t$ denotes the time average. The system is simulated with various electric field strengths, and the current through the nanoslit is measured for each simulation. Error bars are calculated with the standard deviation of the mean. To do this we often simulate the same system with several different initial configurations. A positive electric field is defined as a field that would experimentally be realized by inserting a cathode in the lower ($y < -L/2$) reservoir, while grounding the upper reservoir ($y > L/2$) whereas this is the reverse for a negative electric field.

We will use external electric field strengths of 0.5 to 3 kT/eÅ, or roughly 0.1 to 0.8 V/nm. In a typical system that we will use, which has a total system length of 20 nm, the external field of 3 kT/eÅ corresponds to an applied potential of 15.5 V. This is stronger than the electric fields typically realized in experimental setting, differing by two or three orders of magnitude [19, 34, 56, 109, 110]. Experimental setups usually span micrometers, and data can be collected for hours. In simulations we can only simulate channels with lengths of several nanometers, over a period of time spanning nanoseconds. To be able to collect statistically significant data, higher electric fields are necessary. In line with most simulation studies in this field [42, 44, 95, 102], we therefore work with higher electric fields. Also following the convention in the field of MD simulations of nanotransport, we will report results as a function of the externally applied electric field. In experimental work, the more physical applied electric potential is usually used as a parameter. In simulation studies, however, that would introduce a large dependence on the dimensions of the reservoirs, which complicates comparisons between different studies. It should be noted that the parameter E in this thesis always refers to the externally applied electric field, and not the local electric field, which can vary throughout the channel depending on the width and angle of the channel and the dielectric constant of the spacer wall material.

3.6 Free-Energy Landscapes

To investigate the free-energy costs of travelling through nanochannels, we will calculate Potentials of Mean Force inside these channels. One of the methods that is typically used to measure the potential of mean force in simulations is the Constrained Bias method [111, 112]. To this end we will fix a cation and anion at various positions y along the central axis in the channel, and calculate the average forces that are exerted on them. The free-energy landscape $A(y)$ is related to the reversible work that needs to be done on the ions to drag this ion from the far end of the reservoir to a distance y. Therefore, we will calculate the average forces $\langle F_q^y(y) \rangle_t \equiv \langle \vec{F}_q(y) \rangle_t \cdot \hat{y}$ on an ion of species q at y in the $\hat{y}$ direction, and integrate from the far end y_∞ of the system to y, to obtain the free energy $A(y)$:

$$A(y) = \int_{y_\infty}^{y} dy' \langle F_q^y(y') \rangle_t. \tag{3.12}$$

Numerically we will integrate this from the far end of the reservoir (y_0) using the trapezoid rule to obtain the free energy of ion q at y coordinate y_n

$$A_q(y_n) = \sum_{i=1}^{n} \frac{\Delta y}{2} \big(\langle F_q^y(y_{i-1}) \rangle_t + \langle F_q^y(y_i) \rangle_t \big), \tag{3.13}$$

where $\Delta y = y_{i+1} - y_i$ is the distance between between adjacent sites along the y axis. We recognize that we cannot make our system large enough such that the two ions are far enough apart that their interaction has vanished, as the Bjerrum length in this system is in the order of magnitude of 120 nm [60]. We therefore keep the distance between the cation and anion fixed at a distance of 16 nm. This is half the system size so both periodic images of the ions are at the same distance. We calculate the forces on an ion every 10 fs and output the average every 10 ps for roughly 1 ns in total. This is done for a range of positions throughout the system with steps of 5 Å, such that we get the average forces for both ions at each location in the channel. This is then done for different values of the electric field.

4 Results

4.1 Water Densities

As mentioned in the previous section, we first need to establish the water density in our specific system. Values for this density exist in literature [55], but they have been determined with graphene walls, while we work with LJ 9-3 walls of which the interaction with water is slightly different. It is therefore a reasonable assumption that the correct water density in these slits will also be slightly different. We perform Grand Canonical Monte Carlo calculations as described in Section 3.4. We start the GCMC calculation from the graphene literature value of $\rho = 0.232$ Å^{-2}, at a temperature of 300 K. At first we look at pure water, without any ions.

The water density of this system as a function of time is plotted in Fig. 9(a). We observe that the density becomes constant at roughly $\rho = 0.245$ Å^{-2}. Compared to the initial value of $\rho = 0.232$ Å^{-2}, this is an increase of about 5.6%. This is a relatively minor deviation, but turns out to have big consequences when not taken into account. Unphysical gas bubbles in the water have been observed in nanoslits with LJ 9-3 walls where the water density for graphene slits was used [112]. This was absent for the new value of the water density of $\rho = 0.245$ Å^{-2}. We would also like to perform these calculations in the presence of salt. This will test whether the ions will repel water molecules, attract water, or not affect the number of water molecules at all. We keep the chemical potential of the water constant at $\mu = -10.4$ kcal/mol but besides water molecules, there are also $N_{ions} \in [1, 5]$ ion pairs in the system. Our system in this case has dimensions of 8×4 nm^2 so these values for N_{ions} correspond to ion pair densities of ρ_{ions} between $3 \cdot 10^{-4}$ Å^{-2} (68 mM) and $1.6 \cdot 10^{-3}$ Å^{-2} (365 mM). We perform these calculations for both monovalent ions (sodium chloride NaCl) and divalent ions (calcium sulfate $CaSO_4$).

The results are shown in Fig. 9(b). We show the water density as a function of the ion density. All data points are slightly below the water density without salt of $\rho = 0.245$ Å^{-2}, which corresponds to 781 water molecules in this system. From this data it could be argued that the presence of a divalent salt pushes out more water molecules than a monovalent salt. There does however not seem

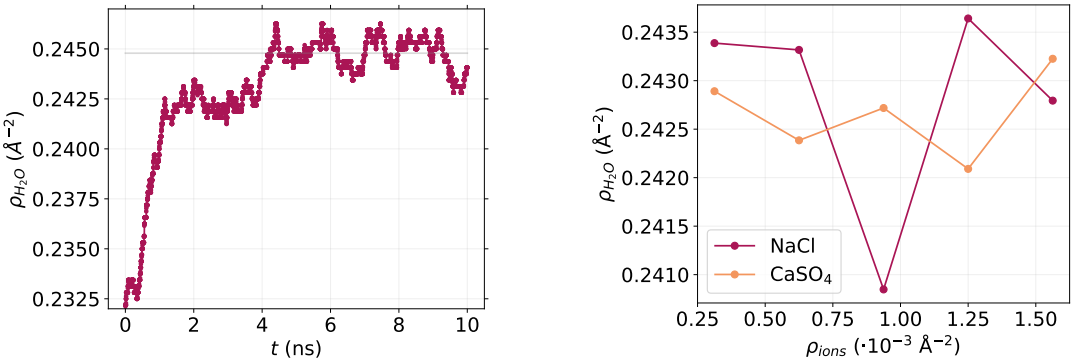

(a) (b)

Figure 9: (a) Water density ρ_{H_2O} (red) during the GCMC calculation with a chemical potential $\mu = -10.4$ kcal/mol in a nanoslit with LJ 9-3 walls without any salt present as a function of time t. The average density of the last 4 ns, $\rho_{H_2O} = 0.245$ Å^{-2} is shown in grey. (b) Density of water ρ_{H_2O} in our system as a function of the ion density ρ_{ions} obtained from GCMC calculations. These values were calculated in a small system of 8×4 nm^2.

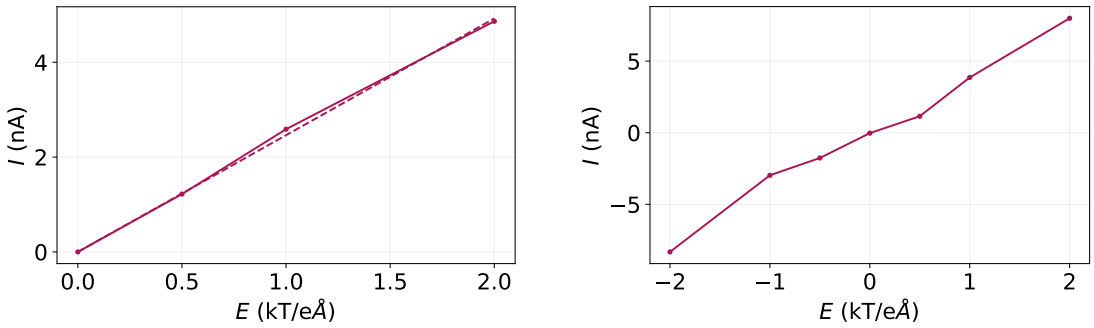

(a) (b)

Figure 10: Ionic current of (a) NaCl (solid) and its Ohmic fit (dashed), with $D_+ + D_- = 1.5 \cdot 10^{-9}$ m^2/s, and (b) $CaSO_4$ with a concentration of $\rho = 7 \cdot 10^{-4}$ Å^{-2}, as a function of the external electric field. This range includes negative electric fields to show the non-linearity, and to show that the currents are symmetric for positive and negative electric fields in this system.

to be a general trend in this data larger than the noise. Fluctuations are to be expected due to the small system size. Deviations from the value of $\rho = 0.245$ Å^{-2} are still less than 0.7% (except for the system with $CaSO_4$ with $\rho_{ions} \approx 0.9$ Å^{-2}, where it is slightly larger but which we would argue is an outlier). Considering this data, we choose to use fixed a water density of $\rho = 0.245$ Å^{-2} for all further simulations, which will be performed in the canonical ensemble. It seems that ions may push out some water molecules, but this effect also seems to be very small and therefore we can safely ignore it, at least for this range of ion concentrations. As mentioned before, we consider relatively low salt concentrations. If one considers much larger ion concentrations, it is conceivable that the significant interactions between salt and water influences the required water density.

4.2 Currents through Regular Nanoslits

Now that we have established the water density, we can add a salt concentration of $\rho = 7 \cdot 10^{-4}$ Å^{-2} (160 mM), as discussed in Section 3.5. We consider the relatively simple system of a regular nanoslit without any asymmetry. We apply a range of electric fields and measure the ionic current through the channel. The currents of NaCl are shown in Fig. 10(a). As we can see, the current is fully linear. This is expected in the two water layer system that we consider. We can, therefore, fit these currents with a linear, Ohmic, $I - E$ curve. From the Nernst-Planck equation we can derive that

$$I = L_x h \sigma E, \tag{4.1}$$

where L_x is the width of the system, h is the height of the channel and the conductivity σ is given by

$$\sigma = \rho_{ion} e^2 \beta (D_+ + D_-), \tag{4.2}$$

where ρ_{ions} is the ion (volume) density. We fit the sum of the (effective) diffusion constants of the cation and anion $D_+ + D_-$ to the measured currents. From this fit we obtain $D_+ + D_- = 1.5 \cdot 10^{-9}$ m^2/s. We also perform these simulations for the divalent $CaSO_4$, to make a comparison to the results of Robin *et al.* [60] and to see if we observe the same non-linear behaviour. This is shown in Fig. 10(b). Indeed we find a non-linearity that is associated with the ion clustering that is described in Refs. [31, 60], where the fraction of free ions, and thus the conductivity, increases when the magnitude of the electric field increases.

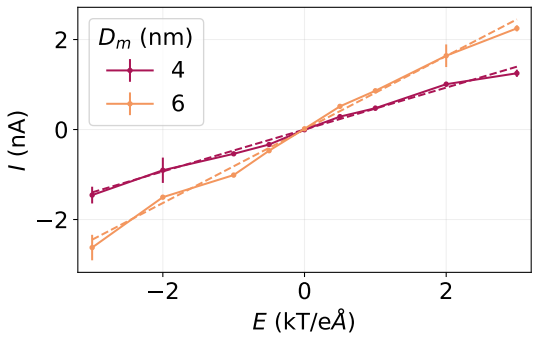

Figure 11: Currents of NaCl through straight channel (with tip-to-base ratio $\xi = 1$) as a function of the electric field E (solid). They are fitted by linear Ohmic curve (dashed) with as fit parameters the diffusion constants $D_+ + D_- = 1.04 \cdot 10^{-9}$ m^2/s for width $D_m = 40$ Å, and $D_- + D_- = 1.21 \cdot 10^{-9}$ m^2/s for width $D_m = 60$ Å.

Considering the fact that there is no asymmetry in the geometry of this nanoslit, it is to be expected that the currents in Fig. 10 are symmetric with respect to the electric field.[4] Just from symmetry arguments, there can be no asymmetry in these currents. This is however not the case in the system with the tapered side walls. We will use the symmetric nanoslit as a reference to compare to an asymmetric system. We expect that the NaCl currents will remain linear since the tapered geometry should not influence clustering behaviour. However, there could be a non-linearity near $E = 0$ if the currents are asymmetrical, as sketched in Fig. 3(a).

4.3 Currents through Tapered Nanoslits

We compare this to the straight channels, where the side walls are explicitly simulated, which have a tip-to-base ratio $\xi = 1$. We look at NaCl in channels with a width $D_m = 40$ Å and $D_m = 60$ Å and plot the currents in Fig. 11. We observe a significantly lower current than those in Fig. 10(a), where there was no lateral confinement. We again fit this with an Ohmic $I - E$ relation which is also plotted in Fig. 11, and seems to be a reasonable approximation to the currents in this case. From this fit we obtain the diffusion constants $D_+ + D_- = 1.04 \cdot 10^{-9}$ m^2/s for width $D_m = 40$ Å, and $D_- + D_- = 1.21 \cdot 10^{-9}$ m^2/s for width $D_m = 60$ Å. These are significantly lower than the diffusion constants of NaCl in nanoslits without lateral confinement.

We now focus on systems that have tapered side walls. We will start with NaCl, and simulate systems with a mean width $D_m = 40$ or 60 Å, and tip-base ratios $\xi = 0.25$ and 0.5. The number of ions in a system is not dependent on ξ, as the mean width of the channel stays the same. This means that we can directly compare currents with the same D_m, but with different ξ. We do this for $D_m = 40$ Å in Fig. 12(a) and for $D_m = 60$ Å in Fig. 12(b). A few things immediately stand out; first of all, the ion current seems slightly non-linear for $E < 0$ when $D_m = 40$ Å. This is a small effect, however. We also see that small asymmetries arise. Actually, for all systems simulated in Fig. 12, we see that the magnitude of the current, and hence the conductivity, is larger for negative electric fields than for positive electric fields. This effect seems to be of the order of 10-20%. This is an appreciable, albeit relatively small, asymmetry.

[4]Mathematically speaking this could better be characterized as 'antisymmetric', as the currents pick up an additional minus sign when flipping the electric field. However, this terminology would become confusing very quickly, as we would then be looking for 'not-antisymmetric' currents. Instead we refer to currents as 'symmetric' when the magnitude of the current is equal for positive and negative currents, and as 'asymmetric' when that is not the case.

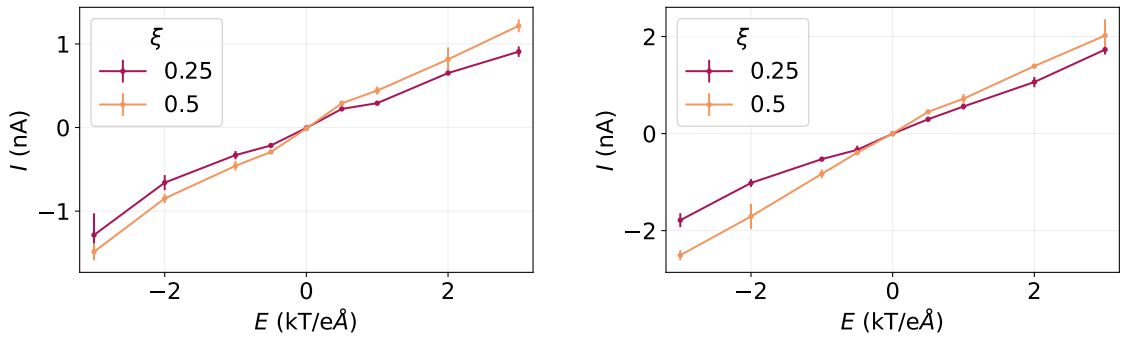

(a) (b)

Figure 12: Currents of NaCl through tapered geometries, with base-tip ratios of $\xi = 0.25$ and 0.5 and with a mean width (a) $D_m = 40$ Å and (b) $D_m = 60$ Å.

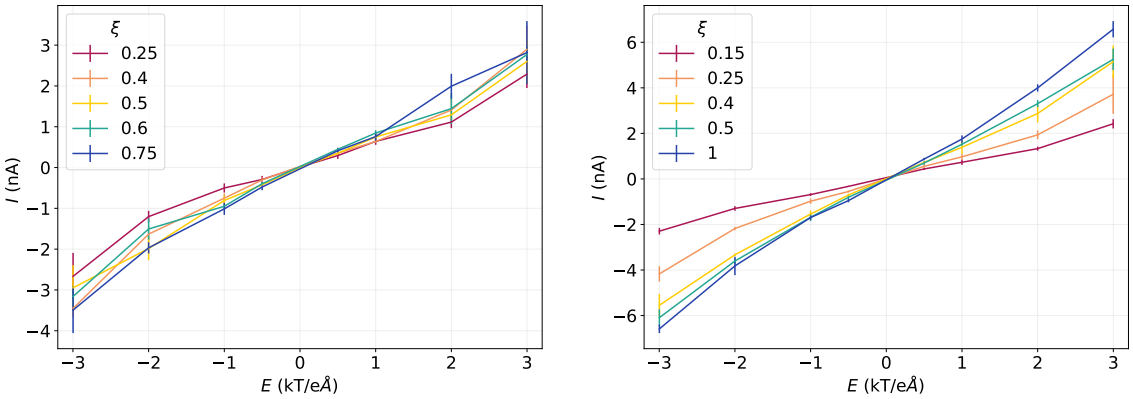

(a) (b)

Figure 13: (a) Currents of (a) $CaSO_4$ and (b) $CaCl_2$ in a tapered geometry with a width $D_m = 60$ Å. The standard deviations of the data are smaller for $CaCl_2$, which is to be expected since it has two anions for every cation, and therefore has 50% more ions than $CaSO_4$ at the same salt concentration.

In order to further investigate the small asymmetries in the currents in tapered channels, we try to replicate it with two different salts: divalent $CaSO_4$ and unibivalent $CaCl_2$. This will tell us something about its generality; whether it is present in all types of salt, or whether it is specific to NaCl. We therefore perform the same simulations with $CaSO_4$ and $CaCl_2$, and do this for a wider range of ratios ξ. The resulting I-E relations are shown in Fig. 13. We, similarly, find small asymmetries in both $CaSO_4$ and $CaCl_2$, for various values of ξ. It is also notable that the conductivity at negative electric fields is larger compared to those at positive electric fields for all of these salts, even though the ions that are involved are completely different. If this effect would depend strongly on the mobilities of the ions, one might expect that the relationship between the conductivity and the electric field strength would depend on the specific combination of ion species involved The anions SO_4 and Cl, and cations Ca and Na have different mobilities, and yet we see a larger conductivity for negative electric fields for all considered combinations.

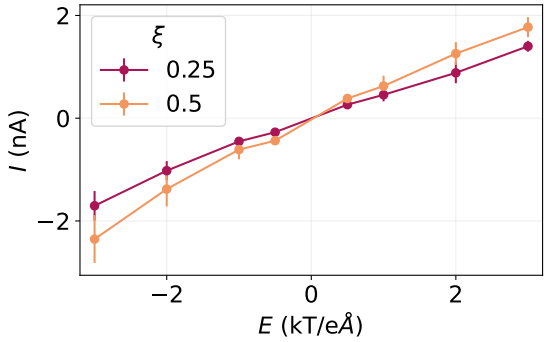

Figure 14: Currents of $X^{2+}Y^{2-}$ through a tapered system with mean width of $D_m = 60$ Å, and with different tip-to-base ratios ξ.

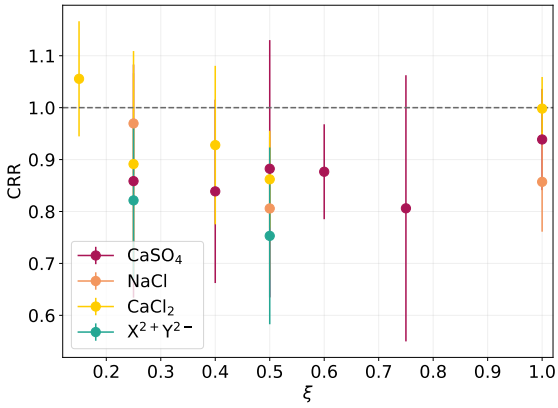

Figure 15: Current Rectification Ratio, CRR, as a function of the tip-to-base ratio ξ, with a mean width of $D_m = 60$ Å, for various salts as labeled.

To further test whether the Lennard-Jones parameters of the ions are of importance to this phenomenon, we also introduce a generic salt $X^{2+}Y^{2-}$, the ions of which have the exact same masses and LJ parameters (see Appendix A) and only differ in the sign of their charge. We again run simulations, this time with this generic salt, and plot the resulting currents in Fig. 14. Surprisingly, we again observe a similar asymmetry. This means that the asymmetry in the current is not contingent on an asymmetry in the LJ parameters, or the masses of the ions; apparently the only import factor is the sign of the charge of the ions.

To quantify the asymmetry in these currents, we introduce the Current Rectification Ratio, which is defined as the ratio between the currents for positive and negative electric field of magnitude $|E| = 3$ kT/eÅ:

$$\mathrm{CRR} = -\frac{I(E = 3\ \mathrm{kT/eÅ})}{I(E = -3\ \mathrm{kT/eÅ})}. \tag{4.3}$$

Clearly, the CRR is unity when the current has the same magnitude for both directions of the electric field, and larger than 1 or smaller than 1 when the positive or negative currents are larger, respectively. We now calculate the CRR for all systems in Figs. 12, 13 and 14 and plot this in Fig. 15. We see that CRR< 1, for essentially all parameters. For very low ξ it is close to 1, and it decreases with increasing

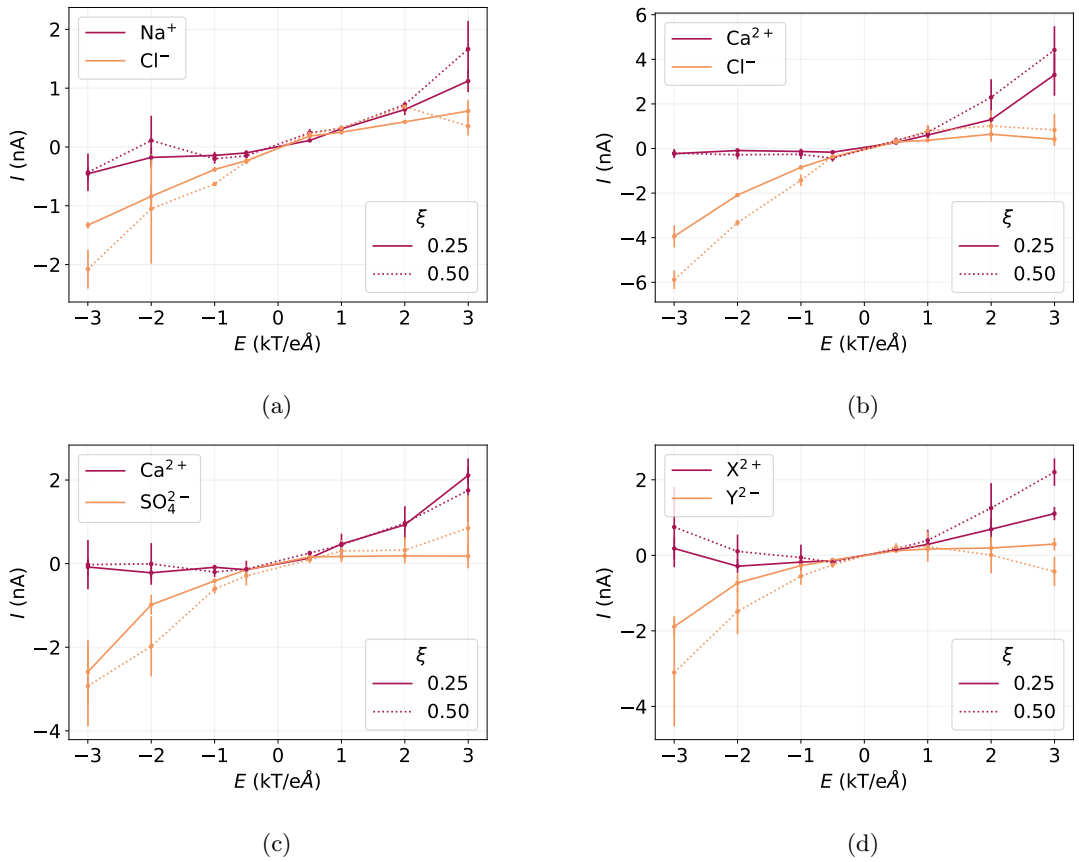

Figure 16: Current contributions as a function of electric field and ξ, for different salts: (a) NaCl, (b) CaCl, (c) $CaSO_4$ and (d) the generic salt XY.

ξ. There may be some sort of minimum, although there is not enough data to be sure of the specific location. For $\xi = 1$, the CRR is on average slightly closer to 1 again. The error of these data points is substantial due to the fact that the relatively large errors of the currents propagate into the CRR. This makes it hard to draw conclusions based on this data, but it is clear that there is a small but consistent effect where negative currents are stronger than positive ones.

4.4 Individual Ion Fluxes

These curious asymmetric currents beg the question how the individual ion species are affected. This may give us some clues as to the origin of this effect. To this end we will calculate the current contributions of the two different ion species, in the same manner that we calculate the entire current, but now calculated per ion species. We also do this for all salts and for both $\xi = 0.25$ and $\xi = 0.5$. This is shown in Fig. 16.

These four plots sketch a very interesting picture. The channel filters either the anions or the cations from the channel depending on the direction of the electric field. This happens for all ion species that we tested, even for the general symmetric $X^{2+}Y^{2-}$ salt. For $CaSO_4$ and $CaCl_2$, the fluxes seem almost completely diodic. One of the ion species barely contributes to the current for one electric field direction and the other species barely contributes when you switch the electric field. This is very different from what you would expect. In a regular nanoslit one would expect both ions to contribute

to the current. They would not necessarily have the same contribution, as their mobilities may be different, but the general trend of the current contributions would be the same for both ions. We show and discuss the current contributions in straight channels in more detail in Appendix B. Another interesting observation is that the current of the anions for negative electric fields is always larger than the current of the cations for positive electric fields. By contrast, as discussed in Section 2, the mobility of anions in a nanoslit is usually lower than that of cations of the same size [42]. When we look at the currents of the generic salt, however, we see that the contribution by Y^{2-} is larger than that of X^{2+}. This does not only mean that the mobility of the ions is strongly dependent on the direction of the electric field, but also that the mobility of negative ions has become larger than that of cations of the same size.

All of this tells us that we should be looking for a mechanism that prevents certain ions from contributing to the current depending on the polarity of the electric field. Not only that, but the required mechanism should also affect the relative mobilities of the cations and the anions in these nanoslits.

4.5 Water Polarization

To further investigate the causes of these asymmetries in the ion fluxes, we will look at the structure of the water, in particular its polarization. Water, whose molecules carry permanent dipoles, can get polarized when an electric field is applied. Dipoles are characterized by the strength of their dipole moment $p = qd$, where q is the displaced charge in the molecule, and d is the displacement of this charge defined from the negative charge to the positive [113]. Water has a dipole moment of $p = 0.389$ eÅ [114]. Due to thermal fluctuations, we will need to perform averages over longer time scales to get reliable data of the average polarization of the water. We collect the following quantity

$$\langle \boldsymbol{P_1}(\boldsymbol{r})\rangle_t = \langle(\cos\theta_x, \cos\theta_y, \cos\theta_z)^T\rangle_t \tag{4.4}$$

where $\theta_{x,y,z}$ is the angle between $\boldsymbol{d}$ and the x, y, z axes , respectively. We collect this data locally in bins of 2×1.5 nm^2 such that we have 100×100 bins throughout the system. This gives us information about both the orientation and overall polarization of the fluid. The polarization $\boldsymbol{P}$ as used in the Maxwell equations is defined as the density of dipole moments and can be calculated with

$$\boldsymbol{P}(\boldsymbol{r}) = p\rho(\boldsymbol{r})\langle \boldsymbol{P_1}(\boldsymbol{r})\rangle_t \tag{4.5}$$

where $\rho(\boldsymbol{r})$ is the local density of dipoles. We run simulations of various system geometries and electric fields. All of these are performed without ions present. We run these simulations for 2 ns, collecting all the coordinates every 100 fs. The dipoles are binned according to the location of the oxygen atom of the water molecule.

The resulting two-dimensional plot of magnitude $|\boldsymbol{P}|$ the polarization field for $E = 3$ kT/eÅ is shown in Fig. 17(a). We see a clear increase of the polarization inside the channel, compared to the reservoirs, where the polarization takes a bulk value of $P = 0.55$ e/nm. This polarization increases when moving upwards through the channel, peaking in the tip of the channel. The polarization does not just point in the y direction, but tends to point toward the opening of the channel. Outside the channel tip, the polarization points nearly radially outwards, as can be seen more clearly in the inset. In Fig. 17(b), a snapshot of the system is shown. It should be noted that not all water molecules point in the average direction as shown in Fig. 17(a), as there are still thermal fluctuations, causing the direction of the water molecules to fluctuate around the preferred direction. To look at the polarization more quantitatively, we plot the magnitude of the polarization along the central axis in Fig. 18. We plot this representation of the polarization in the center of the channel for both directions of the electric field in Fig. 18(a), and we observe no significant differences. This means that the polarization is equal but opposite for the opposite directions of the electric field, as expected. We also plot this for two

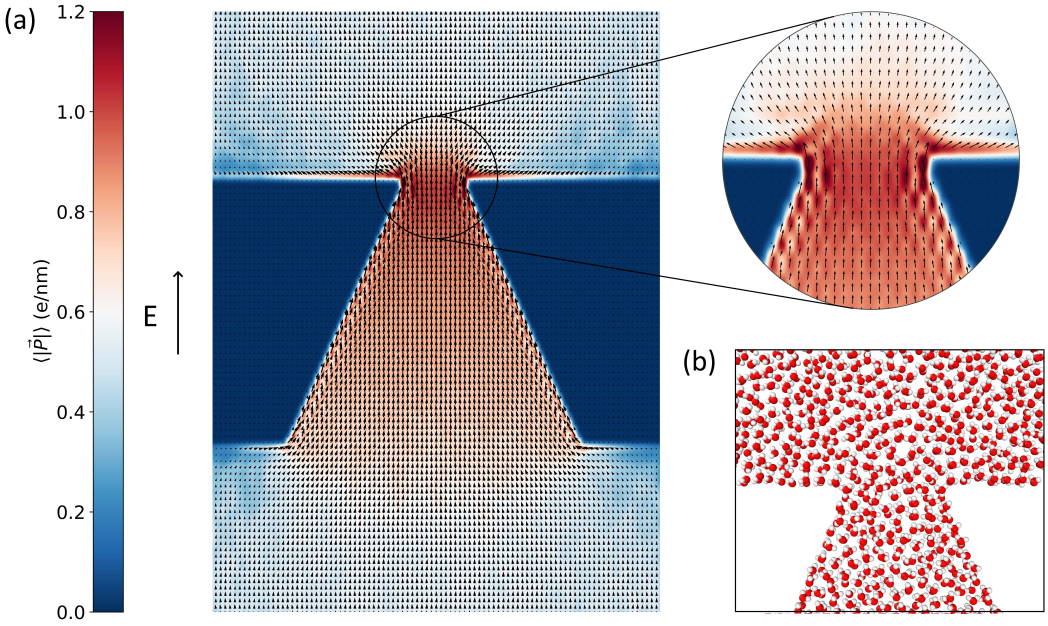

Figure 17: (a) Polarization as calculated with Eq. (4.5), shown as a vector field throughout the system with $D_m = 60$ Å and $\xi = 0.25$. The magnitude of the vector field is shown in the heat map underneath. This system is in equilibrium at an electric field of $E = 3$ kT/eÅ. (b) Snapshot of water molecules in the tip of the channel, taken from the same system.

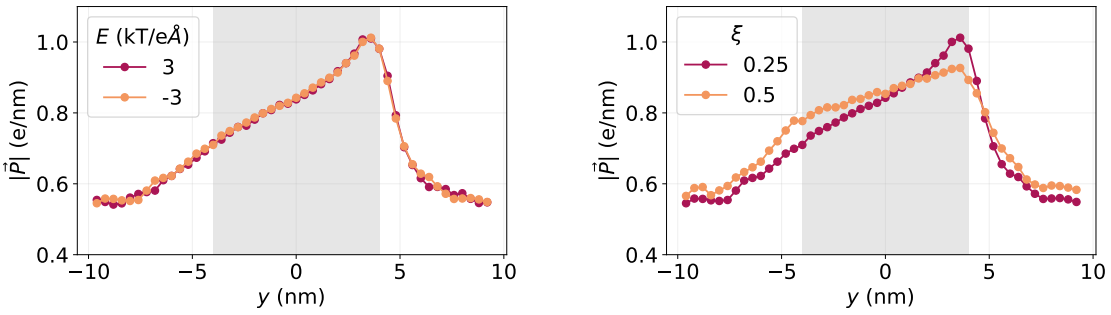

(a) (b)

Figure 18: Magnitude of the polarization along the central y-axis, for (a) electric fields with field strength $E = \pm 3$ kT/eÅ and tip-to-base ratio $\xi = 0.25$, and for (b) values of the tip-to-base ratio $\xi = 0.25$ (red) and $\xi - 0.5$ (orange). In both cases, the mean diameter is $D_m = 60$ Å. The length of the channel is marked in grey where the wide opening is situated at $y = -4$ nm, and the tip at $y = 4$ nm.

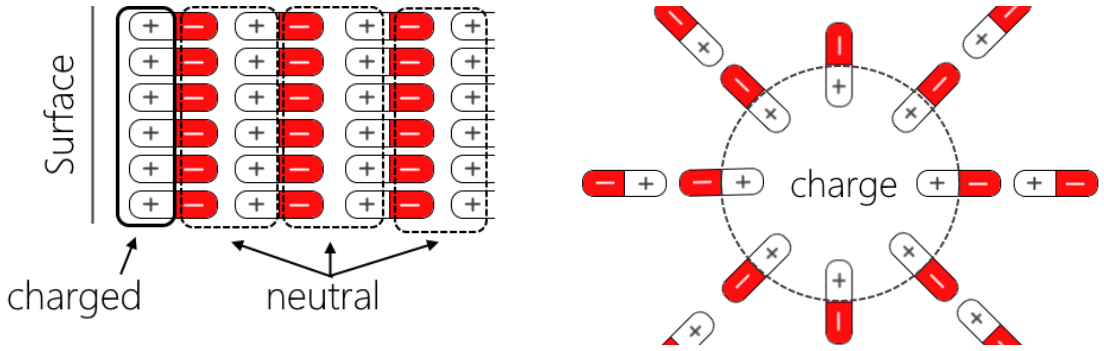

(a) (b)

Figure 19: (a) Sketch of the origin of bound surface charges $\sigma_b = \boldsymbol{P} \cdot \hat{n}$ due to polarization at a surface. At the boundary there is a net charge, while in the bulk the charges are neutralized by other molecules. (b) Sketch of the origin of bound charge in the bulk due to a divergence of the polarization. When there is a divergence, as is the case here in the center, a net charge builds up in that part of the system. Of course, water molecules do not have a net charge so the total bound (surface) charges in the entire system sum to zero as well.

different opening angles of the channel in Fig. 18(b). Here we do see a marked difference between the two cases. The system with $\xi = 0.25$ has a higher polarization around the tip of the channel, while being lower around the base of the channel. This can be explained by the higher electric field in the tip of the $\xi = 0.25$ case due to the pinching of the electric field lines by the tapered side walls.

Looking at these polarization profiles, one might wonder whether this vector field is divergence free. Polarization is dependent on both the electric field – which varies longitudinally due to the pinching of the field lines by the tapered side walls – and the electric susceptibility of the medium – which may be influenced by the changing confinement due to the side wall [29] – so it is conceivable that there are divergences in the polarization. This could have important consequences because divergences in polarization result in a volumetric bound charge distributions:

$$\rho_b = -\nabla \cdot \boldsymbol{P}. \tag{4.6}$$

Moreover, surface polarization gives rise to a bound surface charge density

$$\sigma_b = \boldsymbol{P} \cdot \hat{n}, \tag{4.7}$$

where $\hat{n}$ is the normal vector to the surface. To calculate the bound charges, we make use of the following scheme for the derivatives:

$$\partial_x P_x(x_i) \approx \frac{P_x(x_{i+1}) - P_x(x_{i-1})}{2\Delta x}, \tag{4.8}$$

where ∂_x is the partial derivative in the x direction, x_i is the x coordinate of the bin with index i and Δx is the bin size. Of course this is implemented in the same manner for the y and z directions, and care is taken at the boundaries.

In water, there is no hard boundary of the liquid, as water is not confined to a simple grid, to which we can apply Eq. (4.7). We must first find the distribution of water molecules near the surface. To do that, we calculate the closest distance of all water molecules in the channel to both walls, and plot

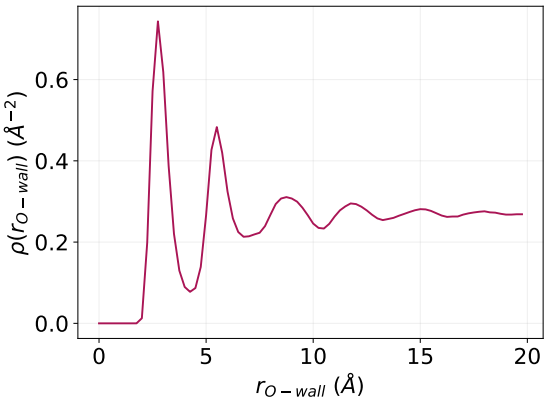

Figure 20: Water density distribution ρ as a function of distance from the spacer walls r_{O-wall}.

their distribution. We use the following equation to find the distance r_{O-wall} between the oxygen atom of a water molecule and the left and right walls:

$$r_{O-wall}(x, y) = \big(x_{wall}(y) \pm x\big) \cos\alpha, \tag{4.9}$$

where α is the angle that the left and right walls make with the y axis, as defined in Section 3.2, x, y are the x and y coordinates of the water molecule and $x_{wall}(y)$ is half the width of the channel at height y, given by

$$x_{wall}(y) = \frac{D_b}{2} - (y + L/2) \tan\alpha. \tag{4.10}$$

Using this, we can plot the distribution of water molecules near the surface. This is shown in Fig. 20. We see that the first minimum is situated at $r_{O-wall} = 4.25$ Å. Everything closer than this belong then on average to the boundary layer of the water, for which Eq. (4.7) holds.

We can now plot the bound charge distributions according to Eqs. (4.6) and (4.7), for $E = -3$ kT/eÅ. We show a map of such a distribution in Fig. 21 and clearly see that there is a bound charge throughout the system, mostly concentrated right outside and inside the tip. The negative charge in the channel itself is more spread out and, therefore, seems to have a lower overall charge density. Besides that, there is quite a surface charge on the reservoir walls. The system should overall be charge neutral, and in this specific case the imbalance of charge is less than 4%, which is reasonable considering the noise in our data and the rather rough grid we used for the computations. All the charge imbalances that we observed are in the range of 0.1-5.4%. As can also be seen in Fig. 21, the data is quite noisy because we are taking numerical derivatives of already noisy polarization data.

It is reasonable to expect that the bound charges in this system have an effect. The positive and negative distributions on both sides of the channel tip add up to charges in the order of magnitude of electron charges. In Fig. 21, a negative electric field has been applied, which means that negative ions would move 'upwards' through the channel and positive ions would move 'downwards'. However, the cations moving downward are repelled by the strong positive bound charge near the opening, making it less likely that it will pass through the channel. The negative ions are slightly repelled by the negative charge right inside the channel, but this distribution is much more spread out, lessening its effects on the ions. This means that anions are more likely to pass through this system than cations, which in turn means that the existence of bound charges in the system is a potential mechanism for the ion selectivity that we observe.

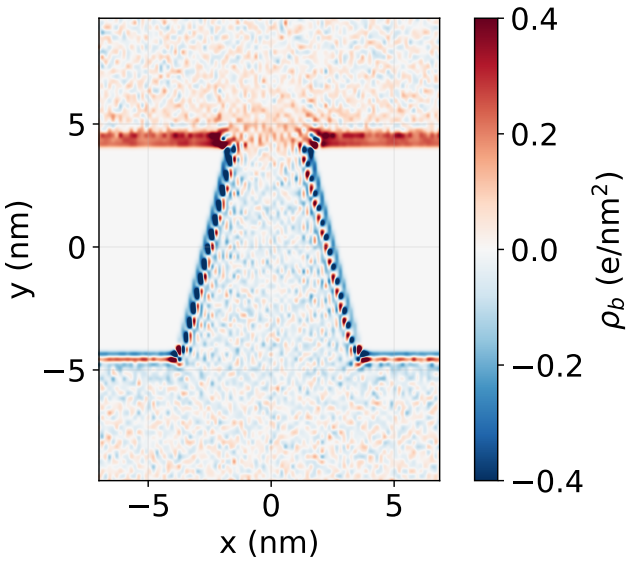

Figure 21: Bound charge distribution ρ_b in a system with a mean width $D_m = 60$ Å and a tip-to-base ratio of $\xi = 0.5$ at an external electric field of $E = -3$ kT/eÅ.

Now that we have established that there is a significant number of bound charges in these systems, we can systematically investigate this effect for multiple electric field strengths and geometries. We perform these calculations for a variety of geometries. First, we take a channel with an average width of $D_m = 60$ Å, and let ξ vary between 0.25 and 1. We plot the bound charge density along the central y axis in Fig. 22. We see that the amount of charge at the tip ($y = 4$ nm) and right inside the channel ($y \approx 2$ nm) decrease with increasing ξ, while the amount of charge at the base ($y < -4$ nm) increases with ξ.

For $\xi = 0.25$, the channel with the smallest tip width, we observe the highest positive charge outside the tip of all of these systems. However, it also has a strong negative charge right inside the channel. The maximum density right outside the tip is about twice that of the oppositely charged region right inside the tip. For systems with higher ξ, the charge outside the channel decreases, and so does the charge inside. It should be noted however, that the ratio between the densities in these regions changes. Where the density outside the tip was twice that of the region inside the tip for $\xi = 0.25$, for $\xi = 0.4$, this is about a factor of three.

We also look at straight channels, with $\xi = 1$. We plot the charge distributions of these systems for various widths D_m in Fig. 23. We see that all of these channels have equal but opposite charge at either end of the channel. Inside these channels, there is barely any charge. The charges at the base and the tip of the channel scale with the width of the channel, and consequently, with the base and tip width. Furthermore, we look at three systems that have the same tip width. In the cases where $D_m = 6$ nm and $\xi = 0.5$ and where $D_m = 4$ nm and $\xi = 1$, the tip width is 4 nm. Not exactly the same, but very similar is the system with $D_m = 8$ nm, and $\xi = 0.3$, which has a tip width of 3.7 nm. We plot the charge distributions for these three systems in Fig. 24. The charge in the channel itself, and near the base ($y < -4$ nm) is completely different in these cases, but the charge near the tip seems comparable in magnitude for these three systems. This is further evidence that the charge densities at the tip scale with the width of the tip.

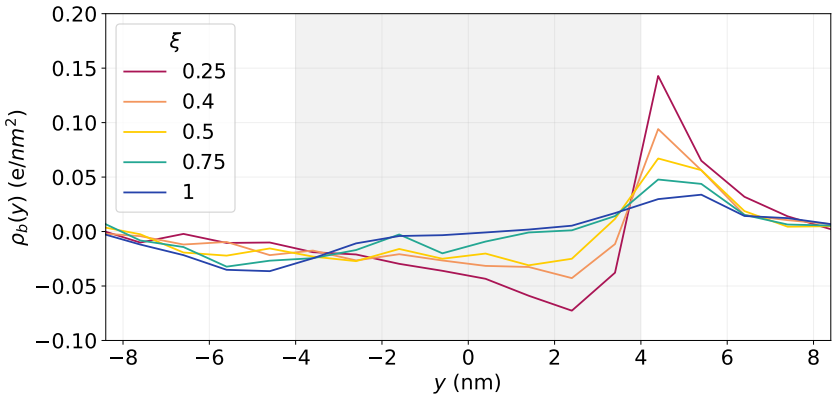

Figure 22: Bound charge density $\rho_b(y)$ along the y axis for different geometries with varying tip-to-base ratios ξ. The systems have a width of $D_m = 60$ Å, and an electric field strength of $E = -3$ kT/eÅ.

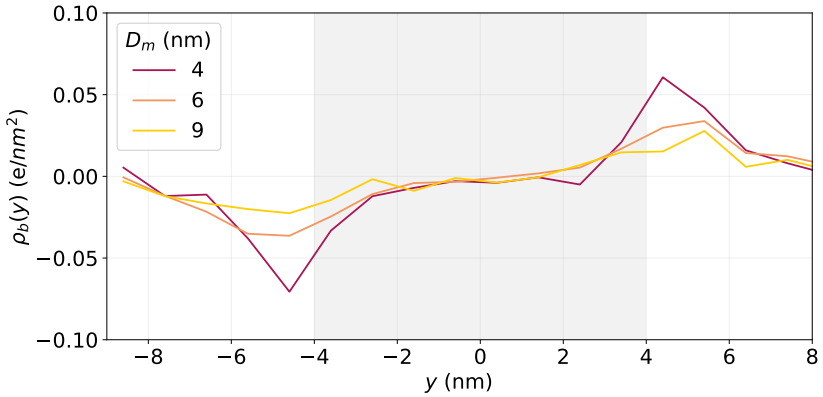

Figure 23: Bound charge density $\rho_b(y)$ along the y axis for straight channels with different widths D_m. The systems have a tip-to-base ratio of $\xi = 1$, and an electric field strength of $E = -3$ kT/eÅ.

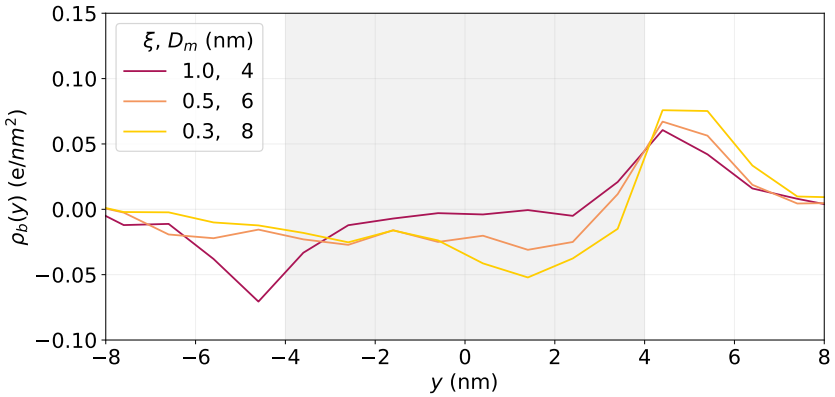

Figure 24: Bound charge density $\rho_b(y)$ along the y axis for three different channel geometries with varying width D_m and tip-to-base ratios ξ such that they all have a tip width of roughly 4 nm. This data was also taken from a run with $E = -3$ kT/eÅ.

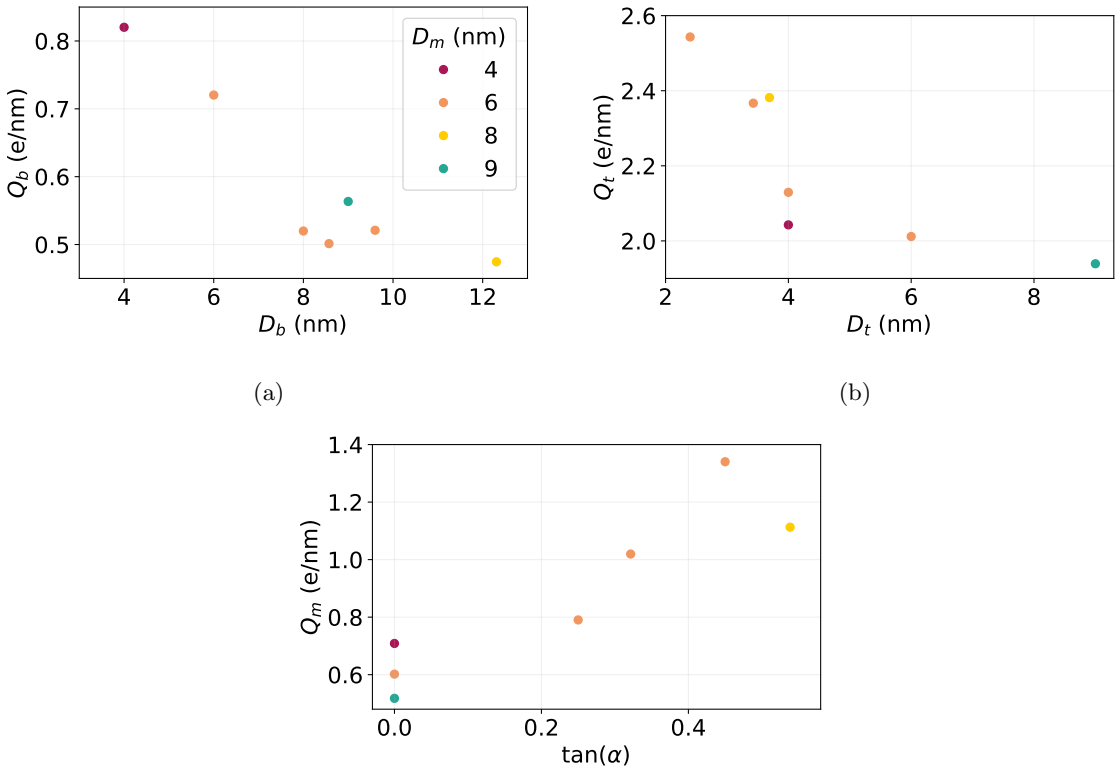

(a) (b)

(c)

Figure 25: (a) Charge Q_b at the base of the channel as a function of base width D_b. (b) Charge Q_t at the tip of the channel as a function of tip width D_t. (c) Charge inside the channel Q_m, as a function of $\tan(\alpha)$.

We further investigate the dependence on the charge distribution in various regions of the channels. We integrate the charge distributions on the central y axis in these regions of interest. We define these regions as follows. The region at the tip is defined to be $y > L/2$, at the base it is defined to be $y < -L/2$ and the charge in the middle is defined to be $-L/2 < y < L/2$. We then plot these integrated charge densities as a function of the aforementioned parameters in Fig. 25. As we can see, there is indeed a correlation between the width of the tip and base and the charge distributions around them. The angle of the channel seems to be correlated to the charge inside. It seems, therefore, that the divergence in the polarization is caused by a change of the width of the channel.

4.6 Free-Energy Landscape

These calculations were done without any ions present. To test whether it will induce any asymmetry in the ionic fluxes, we will now look at the influence that this divergence in the polarization has on ions in these systems. As described in Section 3.6, we will perform Constrained Bias (CB) calculations to obtain the free-energy profile of ions in the tapered system. This is calculated from the average forces on the ions throughout the channel. We do this with the general $X^{2+}Y^{2-}$ salt, because of their identical LJ parameters. We perform these calculations for a tapered nanoslit with a mean width $D_m = 60$ Å and tip-to-base ratios $\xi = 0.25$ and 0.5. If the mechanism behind the described ion selectivity is a static phenomenon (*i.e.* it is still present even when the location of the ions is changed very slowly), then we should be able to see that in the Constrained Bias calculations. This would manifest itself

as a strong decrease of the slope of the Potential of Mean Force of the ions near the entrance of the channel, as well as a decrease in the force on the ions, compared to the reservoir. In Figs. 26-27, we plot the average forces $\langle F \rangle$ divided by the charge of the ions for $\xi = 0.25$ and $\xi = 0.5$. We plot this for both the cations and anions, and for three different electric fields.

This quantity $\langle F \rangle / q$ is usually a measure of the electric field, and so we would expect the lines of the anions and the cations to overlap for all electric fields. This is however not the case. There is a difference between the two ions, which is a signature of a non-electrostatic force. The ions are not equally affected by it. Outside of the tip ($y > L/2$), the force on the cations is larger than that on the anions for $E = 3$ kT/eÅ and smaller for $E = -3$ kT/eÅ. The opposite is true right on the inside of the tip. The maximum is also slightly shifted in position. What we do not observe, however, is a sharp drop in the force just outside of the tip compared to the reservoir. This would be expected if the electrostatic interactions between the polarization-induced bound charges of the water and the ions are the dominating cause of asymmetries in the ion fluxes.

We also plot the actual free energy of ions in a system with $\xi = 0.25$ in Fig. 28. We see that the slopes of the free energy do decrease significantly near the tip ($y > 4$ nm), but never reach zero. This means that the external electric field is strong enough to overcome any repulsion caused by bound charges of the polarized water. Nevertheless, it will most likely contribute to the asymmetry in the ion fluxes. To conclude, there is a small drop in the magnitude of the force when comparing the region just outside of the tip ($y \approx 4$ nm) to the region far away from the tip ($y \approx 16$ nm) of roughly 30%. Similarly, the slope of the free energy decreases in that same area. It is reasonable to expect that this will contribute to the asymmetry in the ion fluxes, up to 30%, but it is then unlikely that it single-handedly causes the almost entirely unidirectional flux that we observe. For that we will need a dynamical mechanism.

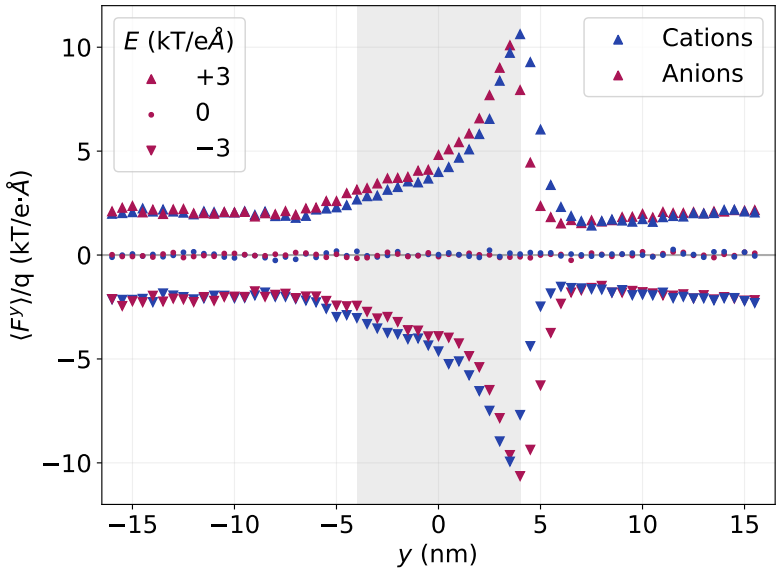

Figure 26: Average forces on ions of both species along the central line of the channel, divided by the ion charge. This quantity is shown for different electric field strengths E. The system has a mean width of $D_m = 60$ Å and tip-to-base ratio $\xi = 0.25$.

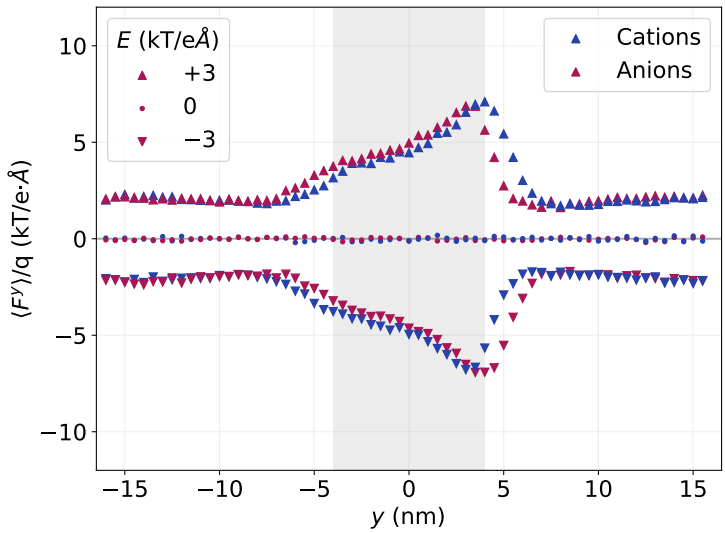

Figure 27: Average forces on ions of both species along the central line of the channel, divided by the ion charge. The system has a mean width of $D_m = 60$ Å and tip-to-base ratio of $\xi = 0.5$.

4.7 Ion Hydration

In other simulation studies, dehydration of the ions has sometimes proven to be a source of asymmetry in currents or ion fluxes [19, 42–44, 110]. These papers investigate much smaller channels than the ones that are considered here and, therefore, we do not expect to see the exact same effects here, but nonetheless it may be interesting to investigate the hydration shells around the ions. We study the hydration number of the $X^{2+}Y^{2-}$ salt along the y axis. This is also called the first coordination number n_1, which is the number of water molecules (binned by the location of its oxygen atom) in the first, closest shell around the ion. We collected this data from the fixed ions in the Constrained Bias runs, so no dynamical effects are taken into account here. We first calculate the radial distribution function, which is shown in Fig. 29, and use that to define the bounds of the first hydration shell. We conclude that everything within $r < 3.2$ Å belongs to the first shell. The first coordination data is then plotted in Fig. 30. We see two minor effects; first, the first hydration shell around the cation, gains on average about 0.4 water molecules in the tip of the channel. The anion on the other hand, loses on average about 0.2 water molecules. These are, however, very minor effects, as the extra hydration of the cation constitutes less than 5% of the first hydration shell, and the dehydration of the anion is less than 2.5%. When dehydration was previously reported to cause any asymmetry, the dehydration could be more than 40% [43, 44].

As we are currently looking at divalent ions, we also look at the second coordination number, defined as the number of water molecules in the second shell ($3.2\text{Å} < r < 5.5\text{Å}$). Here we do see significant changes in the ion shells as a function of the position inside the channel. Due to the polarization, the shells become anisotropic. To illustrate this, we split the coordination number into two parts: the number of water molecules in the second shell ($3.2\text{Å} < r < 5.5\text{Å}$) in the half-space 'above' the ion ($y > y_{ion}$) and below the ion ($y < y_{ion}$). This is plotted in Fig. 31(a). For the anions, the lower half of the hydration shells gains roughly two water molecules, whereas for the cations it is the upper half that gains roughly three. These changes in the hydration layer are also apparent when we plot the distributions of water molecules around the ions in Fig. 31(b)-(e). It turns out that in the tip of the channel, the water shells are compressed in one direction — *e.g.* in the lower half of Fig. 31(d) we see even hints of a third layer within $r < 5.5$ Å — and more spread out in the other. In the reservoir of

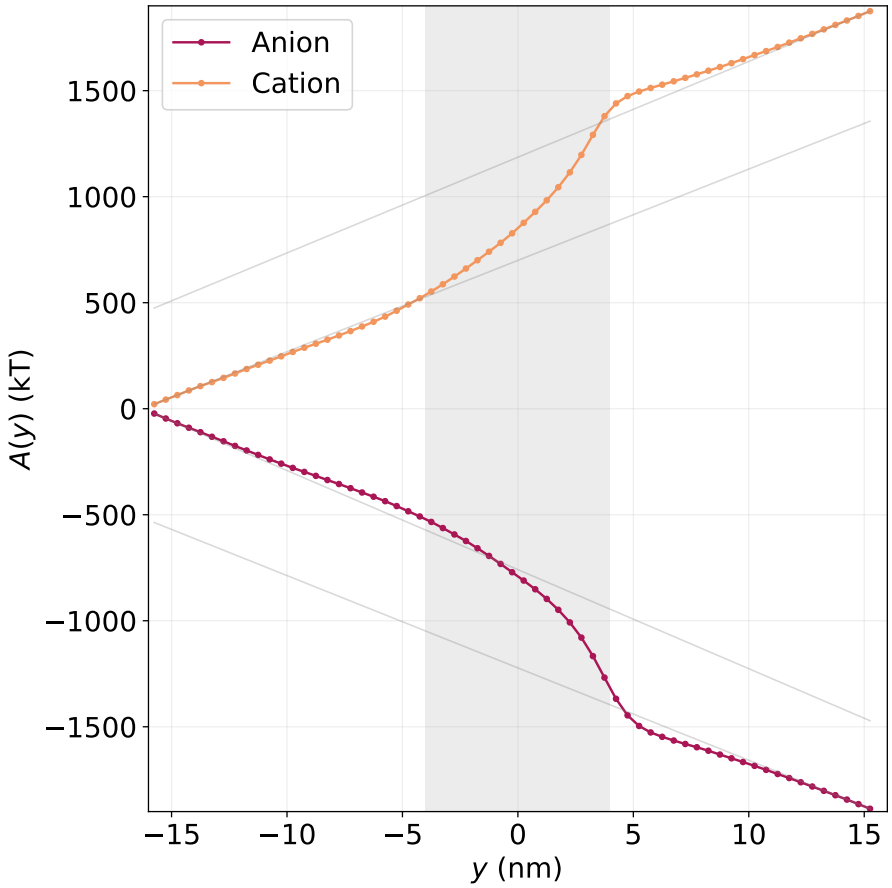

Figure 28: The free-energy profile of the ions through the channel along the central line, shown for both ion species in an electric field of $E = -3$ kT/eÅ. The grey lines indicate the slopes in the far ends of the reservoirs, the grey area signifies the length of the channel. This system has a $D_m = 60$ Å and $\xi = 0.25$. Note the small free energy barriers near $y = 4$ nm and $y = -4$ nm.

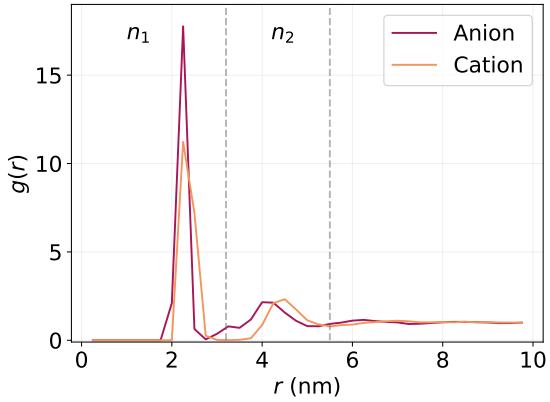

Figure 29: Radial distribution of water molecules (binned by the location of their oxygen atom) around ions of both species at $E = 0$. Calculated from CB data.

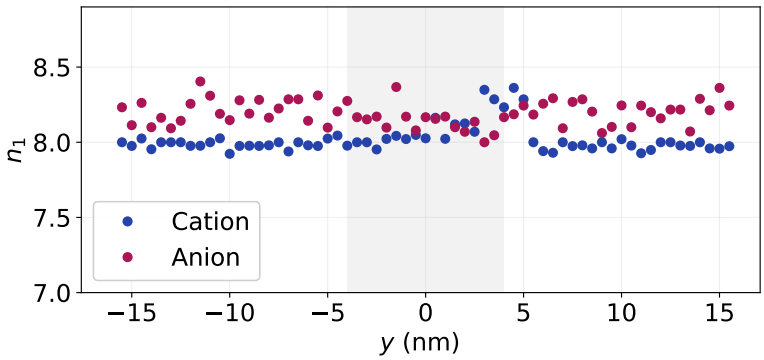

Figure 30: First coordination number n_1 as a function of y along the central line through the channel at $E = 3$ kT/eÅ. The system has a mean width of $D_m = 60$ Å and a tip-to-base ratio $\xi = 0.25$

the system (Fig. 31(b)-(c)), the water forms nearly concentric rings around the ions.

It is not completely unexpected that an ion in a polarized fluid will have anisotropic hydration layers. The preferred orientation of water molecules around an ion will either align or anti-align with the external polarization of the water. Water molecules prefer to point their oxygen atoms towards a cation, for instance, but on one side of the cation this will be in conflict with the polarization due to the external electric field. In the first hydration layer, the electric field due to the ion's charge will be much stronger than the external electric field, and thus we do not see big changes in the first hydration layer. The second hydration layer, however, is further removed from the ion, and is thus less affected by its charge. The consequence is that there will be a repulsive region on that side of the ion as the direction of the water molecules anti-aligns with the preferred orientation with respect to the ion. The water molecules around the cation usually have their oxygen atom pointed towards the ion, but in the lower half of the second hydration shell they point the other way, thereby creating a repulsive force between them. The opposite happens at the other end of the ion; the interaction between the water and the ion is more attractive, as the water molecules are already favorably aligned due to the external field. It is then to be expected that this effect, the anisotropy of the second hydration shell and the consequent force on the ions, scale with the local polarization of the water. This hypothesis is supported by the fact that the anisotropy as plotted in Fig. 31(a) seems highly correlated with the polarization as plotted in Fig. 18(a).

The forces that are exerted on the cations and anions are roughly equal in a homogeneous polarization field. There are differences in the structure of the hydration layers for oppositely charged ions [93], but as we see in Fig. 26 and 27, the difference between the forces on the cations and anions vanishes far away from the channel. We can conclude that these intrinsic differences in structure of the hydration shells only have a minute influence on the force that is exerted on the ions in a homogeneously polarized medium. That is not trivial, however, when there is a divergence in the polarization of the medium. Over a length of 5.5 Å – the radius of the second hydration shell – the polarization changes significantly in the tip of the channel, as can be seen in Fig. 18(a), and to a lesser extent near the base of the channel. That means that the water molecules on the two sides of the ion experience a different external polarization, one stronger than the other. That could conceivably introduce an interaction that is not the same for both ion species. If this mechanism is responsible for the observed differences in the forces of the two ion species, then we expect that this difference in the force $\Delta F^y = |F^y_{anion}| - |F^y_{cation}|$ is proportional to the divergence of the polarization. This difference is plotted in Fig. 33, and indeed it qualitatively matches the divergence of the polarization as plotted in Fig. 22.

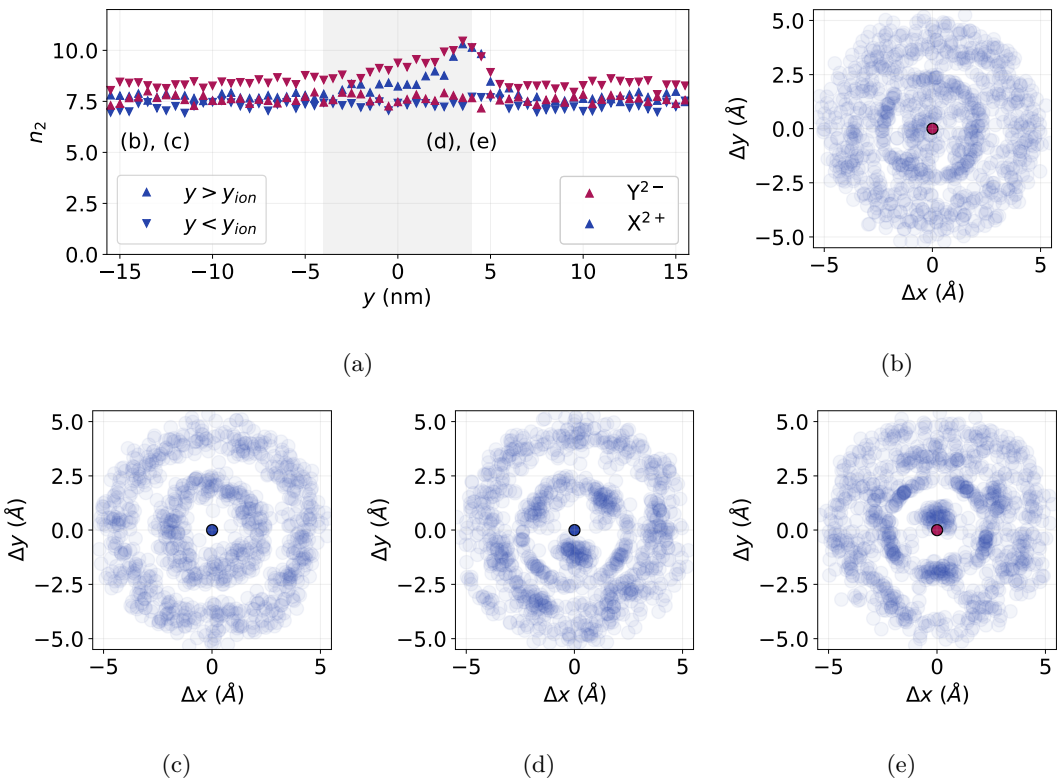

Figure 31: (a) Second coordination number n_2 of cations and anions along the central line of the channel, split between the coordination number of the space above ($y > y_{ion}$) and below ($y < y_{ion}$) the ion. Calculated in system with $D_m = 60$ Å and $\xi = 0.25$ with $E = 3$ kT/eÅ. The channel length is marked by the grey area. (b)-(e) Average distribution of the oxygen atoms of water molecules around the ions: (b) anion in the reservoir ($y = -12$ nm). (c) Cation in the reservoir ($y = -12$ nm). (d) Cation in the tip of the channel ($y = 4$ nm). (e) Anion in the tip of the channel ($y = 4$ nm).

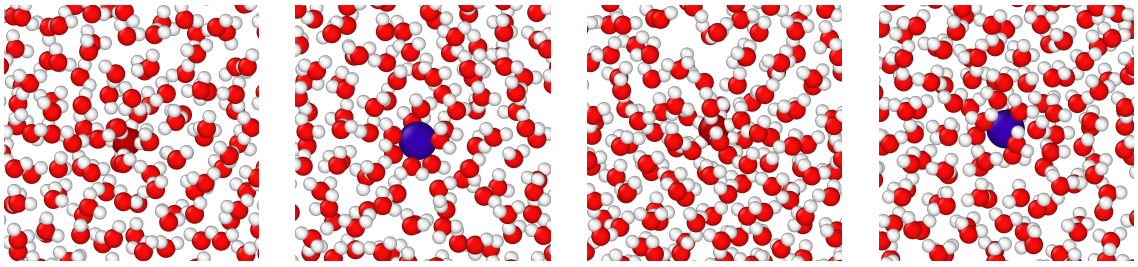

Figure 32: Snapshots of anions (red) and cations (blue) surrounded by water molecules. (a) Anion in the reservoir ($y = -12$ nm) (b) Cation in reservoir ($y = -12$ nm) (c) Anion in the tip of the channel ($y = 4$ nm) (d) Cation in tip of the channel ($y = 4$ nm)

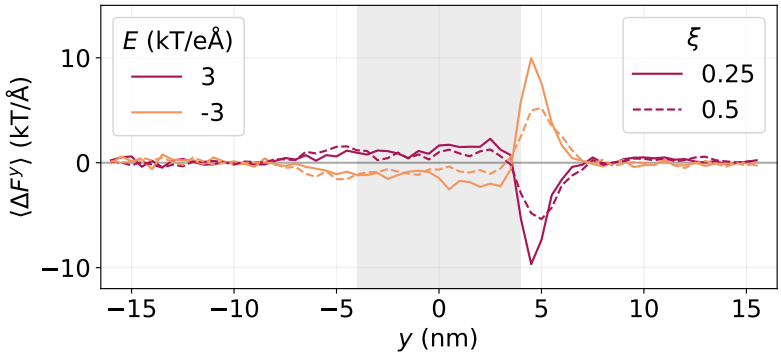

Figure 33: The difference in the forces $\Delta F^y = |F^y_{anion}| - |F^y_{cation}|$ that are exerted on the the cation and anion, as a function of position y along the central axis. Two different systems with tip-to-base ratios ξ are considered. Both have a mean width $D_m = 60$ Å.

4.8 Water flux

Considering that so far, we are missing a dynamical phenomenon that significantly affects the ions, we will look into the dynamical behaviour of the water more closely. Water flow is significantly affected by confinement, and exhibits exotic behaviour in nanochannels and slits. For instance, it was observed that the water fluxes through carbon nanotubes were unexpectedly high when external pressure gradients were applied [32]. In another study, it was shown that the length of nanopores may influence the flow rates due to the formation or breaking of specific hydrogen bond chains through the channel [115]. In all of these cases, however, there was a driving force present – the pressure gradient – that is expected to cause a fluid flow in bulk too. In our current system, however, that is not the case. As discussed in Section 2.1.2, an electric field can in bulk only cause a fluid flow if there is a free (not-bound) charge distribution in the system. From a continuum description such as the PNPS framework, we do not expect fluid flow in our system. Nevertheless, water fluxes have been previously been reported under strong confinement without any charged regions in the system [43, 102, 116]. In these regimes, water and ions can be so strongly coupled that net salt fluxes in one direction may cause a net flux of water molecules as well. We calculate the flux of water molecules in the system and plot them in Fig. 34 for systems containing NaCl and the generic divalent salt XY, respectively. These fluxes are calculated at the middle of the channel $y = 0$, but are constant through the entire system.

We observe that there are very high water fluxes through these systems. The flux is highest for a tip-to-base ratio $\xi = 0.5$ where it reaches 2000 ns^{-1}, which corresponds to an average water velocity of 5 m/s in the entire system. The fluxes are slightly smaller for $\xi = 0.25$, but still considerable. We also observe higher water fluxes for the monovalent sodium chloride than for the generic divalent salt XY. Besides differences between different geometries and salts, we also notice a difference for the different directions of the electric fields. Negative electric fields consistently produce higher water fluxes than positive fields, even in systems with the X^{2+} and Y^{2-} ions, that differ from each other only in the sign of their charge. This is consistent with our findings on the ion fluxes, which were stronger for negative electric fields as well. Additionally, we have seen in Section 4.7 that there are more water molecules in the hydration shells of anion than in the shells of cations, which could lead to a stronger coupling between the movement of water and ions, and could explain the higher water fluxes for negative electric fields.

It should also be noted that the direction of the water flux is the same for both directions of the electric field. This is remarkable, as most fluxes that are observed in nanofluidics are proportional

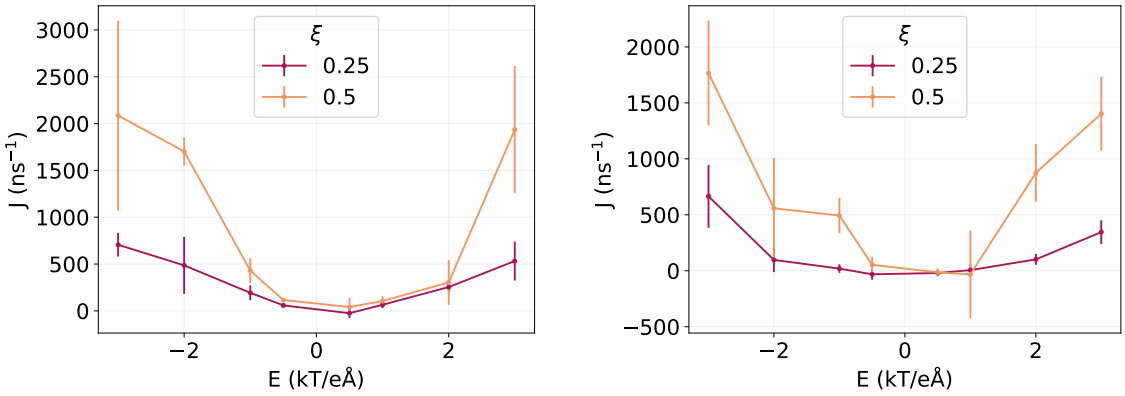

(a) (b)

Figure 34: Water flux J as a function of the external electric field in the systems, which also contain (a) NaCl (b) the generic divalent salt XY. Two different geometries with different tip-to-base ratios ξ are considered.

to their driving forces. When we look at the Stokes equation (Eq. (2.2)), that describes the fluid flow in a more macroscopic regime, we see for instance that the fluid flow is linear in the electric field and pressure gradient. Here this is not the case. The important questions now are: what are the consequences of this fluid flow, and what causes it?

To investigate the extent to which these water fluxes can influence the movement of the ions, we will approximate the advective ion flux J_{adv} that would be associated with a water flux J_{H_2O}. This corresponds to the advective term in the Nernst-Planck equation (Eq. (2.3)), which can be written as:

$$J_{adv} = J_{H_2O} \frac{\rho_{salt}}{\rho_{H_2O}}, \tag{4.11}$$

where ρ_{salt} and ρ_{H_2O} are the overall salt and water densities in the system. For example, we consider

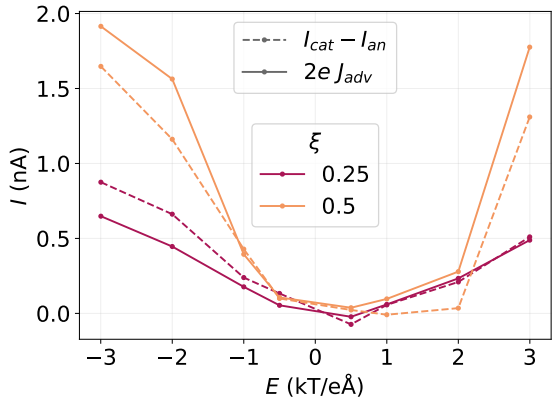

Figure 35: The difference of the current contributions of cations and anions $I_{cat} - I_{an}$ (dashed) and the approximation of the advective component of this difference $2eJ_{adv}$ (solid), shown as a function of the electric field E, for two different tip-to-base ratios ξ. The mean width of the systems is $D_m = 60$ Å.

a flux $J_{H_2O} = 2000$ ns^{-1} that corresponds to a system with $\xi = 0.5$ and $E = -3$ kT/eÅ. We then find an ion flux $J_{salt} = 5.74$ ns^{-1}. If we consider NaCl, this corresponds to an ion current contribution of $\pm eJ_{adv} = \pm 0.9$ nA for both ion species, which is in the order of magnitude of the NaCl ion fluxes measured in Fig. 16. Not only is it in the same order of magnitude, it is about half the difference between the fluxes of the cations and the anions. Both ion species get a current contribution eJ_{adv}. For the ions moving against the flow, this lessens their contribution to the current with eJ_{adv}, while it increases the current contribution with eJ_{adv} of the ion species that moves with the flow. The total current is therefore not affected. To analyze this for all electric fields, we plot both our approximation of the advective current contributions $2eJ_{adv}$ from the water fluxes, together with the difference in current contributions of the cations and anions $I_{cat} - I_{an}$. This is shown in Fig. 35. There is a very good agreement between our approximation of the advective current contributions based on the water flux, and the actual current contributions. The approximation is quite crude as it assumes a homogeneous fluid flow that is independent on ion movement, but we are limited by the dynamical nature of the fluid flows, and a large noise in the data. This approximation does suggest, however, that the diodic ion fluxes that we observed are largely caused by the fluid flow in the system.

It has been shown before in MD studies that ion and water fluxes are strongly correlated in confinement [102, 116]. We have also shown in Section 4.4 that there is a large asymmetry in the ion fluxes, and that there are almost exclusively fluxes going in the positive y direction. This is consistent with the fact that the water velocity is also exclusively pointed in the positive y direction, pointing towards the idea that an asymmetric ion flux causes the water flow. The consequence of this water flow in one direction, however, is itself an increase in the asymmetry of the ion fluxes as we showed in the previous paragraph. Since ions that move in the direction of this water flux will have a significantly higher contribution to the current than those that try to move against it. This may seem like a chicken-and-egg problem, but it may prove to be the final contributing mechanism to the asymmetry of the ion fluxes. We have already pointed out that a divergence in the polarization contributes to the asymmetry in two ways; first of all, there is a bound charge distribution that repels ions that would enter the channel in the $-y$ direction, and secondly, it interacts asymmetrically with the hydration shells of the ions. From the Constrained Bias calculations, however, we concluded that these were not sufficiently strong to cause the full asymmetry. At most, we estimate that they can induce an asymmetry of 30%, not the almost diodic fluxes of Fig. 16. Such a relatively small difference could, however, be big enough of an asymmetry in the ionic flux to cause a water flux. This in turn increases the asymmetry in the ion flux, creating a loop until a steady state forms.

To test this hypothesis, we will investigate the time-dependent behaviour of the ion and water fluxes. We initialize a system with the generic salt XY, a mean channel width of $D_m = 60$ Å and tip-to-base ratio $\xi = 0.25$, without an electric field. Then we turn on the electric field of $E = -3$ kT/eÅ at $t = 0$, and measure the subsequent fluxes. To improve the statistics, we do this with 50 different starting configurations, and take the average over these configurations. We plot the fluxes in Fig. 36. Indeed we see that the cation fluxes are lower from the beginning than the anion fluxes. The cation flux then goes to zero in about 0.13 ns. The anion flux also decreases a little bit, which can most likely be attributed to the enhanced ion cluster formation that happens for $|E| > 0$. We are most interested in the evolution of the water flux, however, but the noise herein is larger than that of the ions. This makes it difficult to draw hard conclusions. We do observe that for $t < 0.13$ ns, the water flux is already strictly positive. It seems also to be on average lower for $t < 0.13$ ns than for $t > 0.13$ ns, and occasionally becomes zero again. which does not happen for $t > 0.13$. All of this does seem to support the hypothesis that an initial asymmetry in the ion fluxes causes a fluid flow. This fluid flow in turn makes the ion fluxes even more asymmetric.

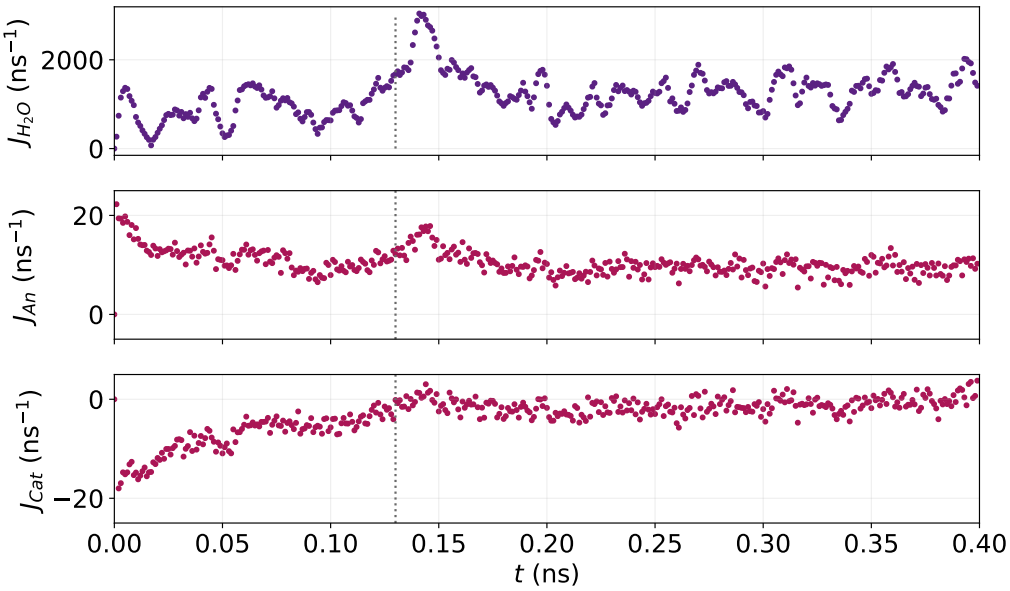

Figure 36: From top to bottom: the water J_{H_2O}, anion J_{an} and cation J_{cat} fluxes, as a function of time t after the electric field has been turned on. The time at which a steady state seems to have been reached is indicated with the dotted line at $t = 0.13$ ns.

4.9 Optimization of Asymmetry

We have now shown that there are both diodic ion fluxes and significant water fluxes. We argue that an initial asymmetry in the ion fluxes is due to the divergence of the polarization of water, and that this causes a fluid flow and consequently a completely diodic ion flux. If this is the case, then we should be able to increase the fluid flow and ion selectivity of the channel by tuning the geometry parameters of the channel. In Section 4.5, we showed that we could control the divergence of the polarization in the channel by changing the tip D_t and base D_b widths and the angle α of the channel. If our hypothesis is correct, we can increase the fluid flow and ion selectivity by increasing the difference in charge density right outside the tip and the charges inside the channel. If we want to lower the charge densities inside and right outside the base of the channel with respect to the charge in the tip, then we need to simultaneously decrease the angle and increase the base width, while keeping the tip width small. This desired combination of a small tip width and a wide base width corresponds to a low value of ξ. Simultaneously, however, we are also looking for a small angle, which seems contradictory. The angle of the channel is given by

$$\tan\alpha = \frac{1-\xi}{1+\xi}\frac{D_m}{L}. \tag{4.12}$$

If we then decrease ξ while keeping D_m/L fixed, we see that indeed the angle increases, which is not what we want. We can, however, simultaneously decrease D_m/L and ξ. As lowering D_m will also make the base smaller, we choose to increase L. To test whether this significantly influences the asymmetry in the currents and fluxes, we will run simulations with $D_m = 60$ Å, $\xi = 0.25$, and increase L from $L = 8$ nm to $L = 12$ nm and $L = 16$ nm.

First, we will simulate this system with only water to obtain data on the polarization and its divergence. This will check whether the predicted relation between the charges and tip widths of Fig. 25 also holds for different channels lengths. We plot the charge distributions through these

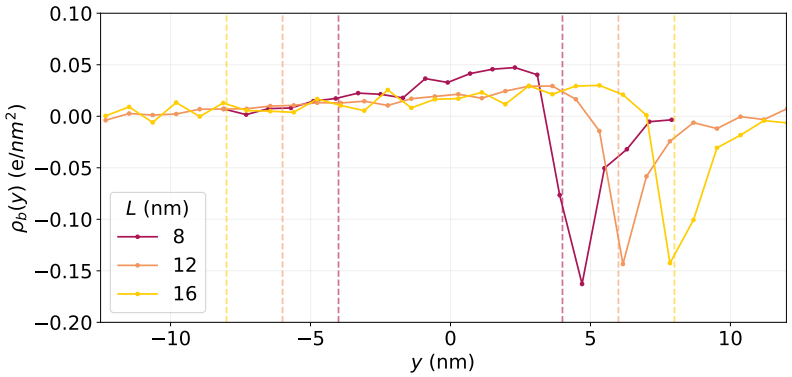

Figure 37: Charge density distributions along the y axis, for systems with various values of L. The area between the dashed lines is inside the channels of these systems.

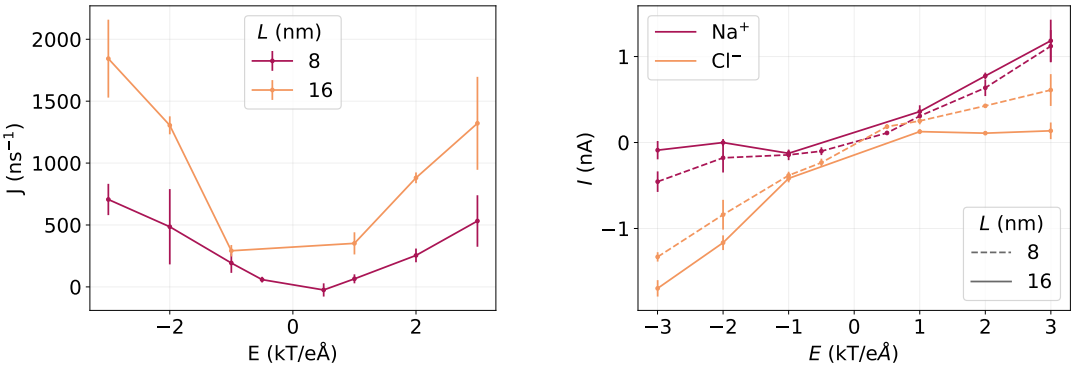

(a) (b)

Figure 38: (a) Water fluxes J and (b) Current contribution of both Na^+ and Cl^-, as a function of the electric field E, for two different geometries with lengths L. Both systems contain NaCl and have a tip-to-base ratio $\xi = 0.25$ and mean width $D_m = 60$ Å.

systems in Fig. 37. We see that the charge right outside of the channel is slightly lower in the longer channels, but the charge density right inside the channel is barely half that of the channel with $L = 8$ nm. Curiously, there does not seem to be a large difference between the channels with lengths $L = 12$ nm and $L = 16$ nm. We do observe a significant drop in the charge density inside the channel, which was exactly what was desired. This means that we expect to see an increase in asymmetry in ion fluxes and currents through these systems.

We now perform simulations in these elongated systems with NaCl ions. We compute the water fluxes and the current contributions of the ions, and plot them in Fig. 38(a) and Fig. 38(b) respectively. We indeed observe a large increase in water flux for $L = 16$ nm compared to the system with $L = 8$ nm. For most electric fields it is an increase by more than a factor of 2. Furthermore, the ion selectivity of the channel is stronger, as can be seen in Fig. 38(b) and the ion fluxes are more diodic in nature.

We also perform these simulations with longer channel lengths with the generic divalent XY salt. Again, we calculate the water fluxes and current contributions, which are shown in Fig. 39. We again

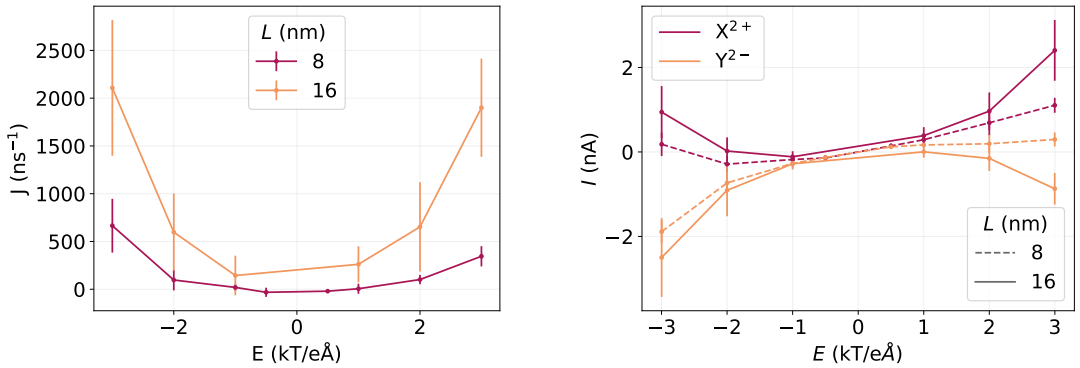

(a) (b)

Figure 39: (a) Water fluxes J and (b) Current contribution of both X^{2+} and Y^{2-}, as a function of the electric field E, for two different geometries with lengths L. Both systems contain the generic divalent salt XY and have a tip-to-base ratio $\xi = 0.25$ and mean width $D_m = 60$ Å.

see a much stronger water flux for $L = 16$. A notable difference from previous simulations, however, is the fact that the water flux seems to be almost symmetric in E in this system. This is in contrast to the other systems which have a larger water flux for negative electric fields $E < 0$. Consequently, we see that the ion fluxes in Fig. 39(b) are also symmetric. Additionally, the fluxes are not diodic anymore, but are somehow reversed, *i.e.* their direction is opposite to the direction that one would expect based on the sign of the electric field. When we inspect these simulations, we observe the formation of large charge-neutral ion clusters – or polyelectrolyes – which are transported through the channel by the fluid flow. This explains the reversing of the ion fluxes, as a large portion of the ion fluxes is actually caused by the transport of these clusters.

Having looked at the ion and water fluxes, we also check whether the longer channel length results in more current rectification. We plot the currents through this elongated systems in Fig. 40. In Fig. 40(a), we see the currents of NaCl, and observe that they are slightly more rectified. For the divalent XY, there is almost no discernible difference in the currents between channels of length $L = 8$ nm and $L = 16$ nm. This is likely the consequence of the symmetric water flux that we observed in Fig. 39. In any case, the current rectification in asymmetric nanoslits seems small in all considered systems.

Overall, it seems that we can tune the selectivity of the channel and the magnitude of the water fluxes through the channel with the geometry parameters. Increasing the channel length – and therefore decreasing the bound charges inside the channel – significantly increases the water flux and ion selectivity.

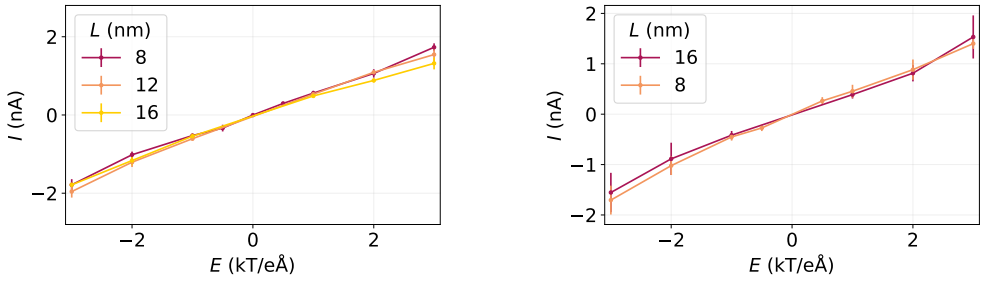

(a) (b)

Figure 40: Currents I of (a) NaCl and (b) the generic divalent salt XY as a function of the electric field strength E, for several channel lengths L.

5 Discussion

In this thesis we set out to investigate ion fluxes in tapered two-dimensional nanoslits. We performed extensive molecular dynamics simulations in various tapered geometries to study ion fluxes, ionic current rectification and water fluxes. All of this is well understood in larger systems with a surface charge (*e.g.* glass cones) [12], but has not yet been observed in the uncharged tapered nanoslits that we studied.

We simulated tapered geometries with various salts, measured the ion currents, and found a small current rectification effect. These systems had at most a Current Rectification Ratio of 0.75, which is a very small effect compared to the CRRs that have been obtained in charged conical nanochannels [65]. The error bars on the CRRs were also quite high, which hindered the identification of the system with the most rectification. More interestingly, however, we found that the ion fluxes through the tapered channels were almost completely diodic. The channel was selective for cations at positive electric fields, and selective for anions for negative electric fields. This was a consistent result for all salts that were tested, and as far as we know, no mechanism to explain the ion selectivity in our channels has been reported in the literature. A previous study has reported a similar ion selectivity effect in a nanoslit with a converging slit height [43], but there the selectivity was attributed to dehydration of the ions and an asymmetric free-energy cost that was associated with it. No such effects occur in our systems, as they are always wide enough for the ions to pass with their hydration shells intact.

We identified and further investigated the polarization – and the divergence thereof – as a potential explanation for the asymmetric ion fluxes. We observed a strong polarization of the water that was mainly situated inside the channel, and seemed to be roughly inversely proportional to the system width. This is in general a result of the low dielectric constant of the tapered spacer layers, as it forces the electric field lines to go through the channel. In our simulation, we use the Lennard-Jones 9-3 potential to simulate the walls of the system, and, hence, the spacer layers have a relative dielectric constant of 1. More elaborate schemes would have to be implemented to take the dielectric constant of the wall materials into account. Another potential factor that could influence the water polarization is the water model that is used. The behaviour of water is crucial to the phenomena that we describe in this thesis. In this thesis we have chosen to use the SPC/E model of water. There is, however, a host of water models, as discussed in Section 3.3, and there may be differences between them, both in structure and in dynamical properties. Due to variations in the water models, the polarization might be weakened or enhanced. Analyzing the consistency of our results for different water molecules might be of interest. Overall, the divergence of the polarization and the resulting bound charge distribution are fascinating phenomena that have – to the best of our knowledge – never before been observed before in nanofluidic systems.

Having identified the divergence of the polarization as a possible source of asymmetry in the ion fluxes, we performed Constrained Bias simulations to test whether it could be entirely responsible for the observed selectivity. The polarization and its divergence are static phenomena, and should therefore give a contribution to the potential of mean force of the ions through the channel. We find relatively small energy barriers for both ion species. For the ions trying to enter the channel from the 'upper' reservoir ($y > L/2$), however, this barrier was about 30% higher. Compared to the very high ion selectivity in this channel, we deemed the asymmetry in the energy barriers too low to be a complete explanation, although it is expected that it does contribute. For a complete explanation we needed a dynamical mechanism.

We observed a large water flux through the system. This flux was more than one order of magnitude larger than those found previously in symmetric graphene nanoslits of similar size [102]. It has been shown before that ion and water fluxes are coupled [43, 102, 116] in confined systems. Given an

asymmetrical ion flux, it is therefore not unexpected that we also find a water flux. We argue that there is an initial asymmetry in ion fluxes due to the divergence of the polarization; that this causes a water flow which in turn amplifies the asymmetry in the ion fluxes. It is, however, very hard to conclusively show this time-dependent behaviour during initialization. Even when averaging over 50 different starting configurations, the statistics were not very good, although it should be said that the results were in rough agreement with our hypothesis. We could potentially get better statistics with NaCl, since monovalent salts do not cluster. Time constraints prevented us from repeating the analysis with NaCl, however.

We tried to increase the asymmetry in the ion fluxes by changing the geometry parameters. Specifically, we tried to lower the bound charge density inside the channel by increasing the channel length L. The bound charge density was indeed lower right inside the channel when the channel had a length of $L = 12$ or 16 nm compared to the density in channels with length $L = 8$ nm, but surprisingly we did not observe significant differences between the systems with $L = 12$ nm and $L = 16$ nm. The correlation between the angle of the channel and the bound charge inside the channel may break down for low charge densities. Due to the overall charge neutrality of water, the bound charge density inside the channel cannot be arbitrarily low since the large charge right outside the tip must be compensated. A more rigorous analysis of the polarization could potentially be very interesting. Research on theoretical models of the dielectric properties of water in these systems could further illuminate the behaviour of the water polarization as a function of the geometry parameters.

Additionally, the fluxes of a system with the generic divalent salt and a channel length of $L = 16$ nm were quite unexpected. For $L = 8$ nm, we always observed higher water fluxes and higher ion fluxes for negative electric fields compared to positive field strengths. When looking at a channel with $L = 16$ nm, however, we see that they are symmetric. Upon inspection, it seems as if there is an increased formation of large ion clusters in this system. We do not know why this happens. In this thesis, we have largely ignored clustering effects, even though they can play a large role in the transport of divalent ions in large electric fields [60]. We have neither investigated the hydration shells of ion clusters, nor the influence of a divergence of the water polarization on them. Furthermore, it is reasonable to expect that the water flux that is caused by polyelectrolytes is more symmetric since polyelectrolytes with an overall charge of ± 1 differ only by one ion, while the entire cluster may be comprised of up to 5 ions. It would be interesting to investigate the clustering behaviour of divalent salts in conjunction with their dynamical behaviour.

As also mentioned in Section 3.5, we performed simulations at unphysically high electric fields. It is hard to predict whether the phenomena that we describe in this thesis will be present with electric field strengths that can be realized experimentally, as the simulation times that would be necessary to collect enough data at realistic electric field strengths are currently not feasible. Experimental studies on this system would, therefore, be of great interest.

6 Conclusion

In this thesis we study the behaviour of water and ions in uncharged asymmetric nanoslits. We systematically performed a large number of simulations with different geometry parameters, electric field strengths and salts, in order to observe asymmetric ion fluxes or currents.

There is ionic current rectification in tapered nanoslits, with a rectification ratio between 0.75 and 0.9. Albeit noticeable, this is not a large effect. The ion fluxes, however, are very asymmetrical. We observe a diodic effect; the channel is almost fully selective for anions in a negative electric field, and selective for cations when a positive field is applied. We attribute this selectivity to a combination of a divergent polarization of the water, and a strong water flux. The divergence of the water polarization leads to a bound charge distribution in the water, which creates a small energy barrier for entering the channel. Furthermore, the water with a divergent polarization interacts asymmetrically with the hydration shells of the ions, thereby creating a difference in the height of the energy barrier of the cation and anion. We show that this leads to a large fluid flow by introducing an asymmetry in the ion flux. This fluid flow consequently increases the asymmetry in ion fluxes until it is fully diodic. To the best of our knowledge, this is a novel mechanism for obtaining ion selectivity that has not been described before in literature. These tapered nanoslits could potentially find interesting applications in the design of biomimetic channels and new nanofluidic devices.

References

[1] D. C. Tosteson and J. F. Hoffman. "Regulation of Cell Volume by Active Cation Transport in High and Low Potassium Sheep Red Cells". In: *The Journal of General Physiology* 44 (1 Sept. 1960), p. 169. ISSN: 00221295. DOI: 10.1085/JGP.44.1.169.

[2] W. Chen and M. Kudryashev. "Structure of RyR1 in native membranes". In: *EMBO reports* 21 (5 May 2020), e49891. ISSN: 1469-3178. DOI: 10.15252/EMBR.201949891.

[3] A. L. Hodgkin and A. F. Huxley. "A quantitative description of membrane current and its application to conduction and excitation in nerve". In: *The Journal of Physiology* 117 (4 Aug. 1952), pp. 500–544. ISSN: 14697793. DOI: 10.1113/JPHYSIOL.1952.SP004764.

[4] D. Voet and J. G. Voet. *Biochemistry*. 4th ed. J. Wiley & Sons, 2011. ISBN: 1118139933.

[5] B. Hille. "Ionic channels in excitable membranes. Current problems and biophysical approaches." In: *Biophysical Journal* 22 (2 1978), p. 283. ISSN: 00063495. DOI: 10.1016/S0006-3495(78)85489-7.

[6] E. Kruse, N. Uehlein, and R. Kaldenhoff. "The aquaporins". In: *Genome Biology* 7 (2 Feb. 2006), pp. 1–6. ISSN: 1474760X. DOI: 10.1186/GB-2006-7-2-206.

[7] *Press release: The Nobel Prize in Chemistry 2003*. URL: https://www.nobelprize.org/prizes/chemistry/2003/press-release/.

[8] W. A. Catterall. "Structure and Function of Voltage-Gated Sodium Channels at Atomic Resolution". In: *Experimental physiology* 99 (1 2014), pp. 35–51. ISSN: 1469445X. DOI: 10.1113/EXPPHYSIOL.2013.071969.

[9] W. Kopec et al. "Direct knock-on of desolvated ions governs strict ion selectivity in K+ channels". In: *Nature Chemistry 2018 10:8* 10 (8 July 2018), pp. 813–820. ISSN: 1755-4349. DOI: 10.1038/S41557-018-0105-9.

[10] C. M. Armstrong and S. Hollingworth. "Na+ and K+ channels: history and structure". In: *Biophysical Journal* 120 (5 Mar. 2021), p. 756. ISSN: 15420086. DOI: 10.1016/J.BPJ.2021.01.013.

[11] N. Kavokine, R. R. Netz, and L. Bocquet. "Fluids at the Nanoscale: From Continuum to Subcontinuum Transport". In: *Annual Review of Fluid Mechanics* 53 (Jan. 2021), pp. 377–410. ISSN: 00664189. DOI: 10.1146/ANNUREV-FLUID-071320-095958.

[12] L. Bocquet. "Nanofluidics coming of age". In: *Nature Materials 2020 19:3* 19 (3 Feb. 2020), pp. 254–256. ISSN: 1476-4660. DOI: 10.1038/S41563-020-0625-8.

[13] K. Celebi et al. "Ultimate permeation across atomically thin porous graphene". In: *Science* 344 (6181 Apr. 2014), pp. 289–292. ISSN: 10959203. DOI: 10.1126/SCIENCE.1249097.

[14] S. Garaj et al. "Graphene as a subnanometre trans-electrode membrane". In: *Nature 2010 467:7312* 467 (7312 Aug. 2010), pp. 190–193. ISSN: 1476-4687. DOI: 10.1038/nature09379.

[15] G. Hummer, J. C. Rasaiah, and J. P. Noworyta. "Water conduction through the hydrophobic channel of a carbon nanotube". In: *Nature 2001 414:6860* 414 (6860 Nov. 2001), pp. 188–190. ISSN: 1476-4687. DOI: 10.1038/35102535.

[16] C. Y. Lee et al. "Coherence resonance in a single-walled carbon nanotube ion channel". In: *Science* 329 (5997 Sept. 2010), pp. 1320–1324. ISSN: 00368075. DOI: 10.1126/SCIENCE.1193383.

[17] A. Siria et al. "Giant osmotic energy conversion measured in a single transmembrane boron nitride nanotube". In: *Nature 2013 494:7438* 494 (7438 Feb. 2013), pp. 455–458. ISSN: 1476-4687. DOI: 10.1038/nature11876.

[18] B. Radha et al. "Molecular transport through capillaries made with atomic-scale precision". In: *Nature 2016 538:7624* 538 (7624 Sept. 2016), pp. 222–225. ISSN: 1476-4687. DOI: 10.1038/nature19363.

[19] A. Esfandiar et al. "Size effect in ion transport through angstrom-scale slits". In: *Science* 358 (6362 Oct. 2017), pp. 511–513. ISSN: 10959203. DOI: 10.1126/SCIENCE.AAN5275.

[20] Z. Siwy et al. "Conical-nanotube ion-current rectifiers: The role of surface charge". In: *Journal of the American Chemical Society* 126 (35 Sept. 2004), pp. 10850–10851. ISSN: 00027863. DOI: 10.1021/JA047675C.

[21] L. Jubin et al. "Dramatic pressure-sensitive ion conduction in conical nanopores". In: *Proceedings of the National Academy of Sciences of the United States of America* 115 (16 2018), pp. 4063–4068. ISSN: 10916490. DOI: 10.1073/pnas.1721987115.

[22] M. Majumder et al. "Enhanced flow in carbon nanotubes". In: *Nature 2005 438:7064* 438 (7064 Nov. 2005), pp. 44–44. ISSN: 1476-4687. DOI: 10.1038/438044A.

[23] F. Fornasiero et al. "Ion exclusion by sub 2-nm carbon nanotube pores". In: *Proc. Natl. Acad. Sci. USA.* 105 (45 Nov. 2008), pp. 17250–17255. ISSN: 00278424. DOI: 10.1073/pnas.0710437105.

[24] G. Laucirica et al. "Shape matters: Enhanced osmotic energy harvesting in bullet-shaped nanochannels". In: *Nano Energy* 71 (May 2020), p. 104612. ISSN: 2211-2855. DOI: 10.1016/J.NANOEN.2020.104612.

[25] R. Karnik et al. "Rectification of ionic current in a nanofluidic diode". In: *Nano Letters* 7 (3 Mar. 2007), pp. 547–551. ISSN: 15306984. DOI: 10.1021/NL062806O.

[26] W. Q. Boon et al. "Pressure-sensitive ion conduction in a conical channel: Optimal pressure and geometry". In: *Physics of Fluids* 34 (10 Oct. 2022), p. 101701. ISSN: 1070-6631. DOI: 10.1063/5.0113035.

[27] V. Kapil et al. "The first-principles phase diagram of monolayer nanoconfined water". In: *Nature 2022 609:7927* 609 (7927 Sept. 2022), pp. 512–516. ISSN: 1476-4687. DOI: 10.1038/s41586-022-05036-x.

[28] A. Schlaich, E. W. Knapp, and R. R. Netz. "Water Dielectric Effects in Planar Confinement". In: *Physical Review Letters* 117 (4 July 2016), p. 048001. ISSN: 10797114. DOI: 10.1103/PHYSREVLETT.117.048001.

[29] L. Fumagalli et al. "Anomalously low dielectric constant of confined water". In: *Science* 360 (6395 June 2018), pp. 1339–1342. ISSN: 10959203. DOI: 10.1126/SCIENCE.AAT4191.

[30] N. R. Aluru and M. H. Motevaselian. "Universal reduction in dielectric response of confined fluids". In: *ACS Nano* 14 (10 Oct. 2020), pp. 12761–12770. ISSN: 1936086X. DOI: 10.1021/ACSNANO.0C03173.

[31] W. Zhao et al. "Two-dimensional monolayer salt nanostructures can spontaneously aggregate rather than dissolve in dilute aqueous solutions". In: *Nature Communications 2021 12:1* 12 (1 Sept. 2021), pp. 1–8. ISSN: 2041-1723. DOI: 10.1038/s41467-021-25938-0.

[32] J. K. Holt et al. "Fast mass transport through sub-2-nanometer carbon nanotubes". In: *Science* 312 (5776 May 2006), pp. 1034–1037. ISSN: 00368075. DOI: 10.1126/SCIENCE.1126298.

[33] K. Falk et al. "Molecular origin of fast water transport in carbon nanotube membranes: Superlubricity versus curvature dependent friction". In: *Nano Letters* 10 (10 Oct. 2010), pp. 4067–4073. ISSN: 15306992. DOI: 10.1021/NL1021046.

[34] E. Secchi et al. "Scaling behavior for ionic transport and its fluctuations in individual carbon nanotubes". In: *Physical Review Letters* 116 (15 Apr. 2016), p. 154501. ISSN: 10797114. DOI: 10.1103/PHYSREVLETT.116.154501.

[35] R. H. Tunuguntla et al. "Enhanced water permeability and tunable ion selectivity in subnanometer carbon nanotube porins". In: *Science* 357 (6353 Aug. 2017), pp. 792–796. ISSN: 10959203. DOI: 10.1126/science.aan2438.

[36] M. Barboiu. "Artificial water channels – incipient innovative developments". In: *Chemical Communications* 52 (33 Apr. 2016), pp. 5657–5665. ISSN: 1364548X. DOI: 10.1039/C6CC01724J.

[37] J. Cervera, B. Schiedt, and P. Ramírez. "A poisson/nernst-planck model for ionic transport through synthetic conical nanopores". In: *Europhysics Letters* 71 (1 July 2005), pp. 35–41. ISSN: 02955075. DOI: 10.1209/EPL/I2005-10054-X.

[38] J. Cervera et al. "Ionic conduction, rectification, and selectivity in single conical nanopores". In: *Journal of Chemical Physics* 124 (10 2006). ISSN: 00219606. DOI: 10.1063/1.2179797.

[39] H. S. White and A. Bund. "Ion current rectification at nanopores in glass membranes". In: *Langmuir* 24 (5 Mar. 2008), pp. 2212–2218. ISSN: 07437463. DOI: 10.1021/LA702955K.

[40] J. A. Thomas, A. J. McGaughey, and O. Kuter-Arnebeck. "Pressure-driven water flow through carbon nanotubes: Insights from molecular dynamics simulation". In: *International Journal of Thermal Sciences* 49 (2 Feb. 2010), pp. 281–289. ISSN: 1290-0729. DOI: 10.1016/J.IJTHERMALSCI.2009.07.008.

[41] R. K. Joshi et al. "Precise and ultrafast molecular sieving through graphene oxide membranes". In: *Science* 343 (6172 2014), pp. 752–754. ISSN: 10959203. DOI: 10.1126/science.1245711.

[42] Y. Yu et al. "Dehydration impeding ionic conductance through two-dimensional angstrom-scale slits". In: *Nanoscale* 11 (17 Apr. 2019), pp. 8449–8457. ISSN: 20403372. DOI: 10.1039/C9NR00317G.

[43] S. Li et al. "Rectification Correlation between Water and Ions through Asymmetric Graphene Channels". In: *Journal of Physical Chemistry B* 125 (40 Oct. 2021), pp. 11232–11241. ISSN: 15205207. DOI: 10.1021/ACS.JPCB.1C05255.

[44] S. Li et al. "Asymmetric transport and desalination in graphene channels". In: *Physical Chemistry Chemical Physics* 24 (21 June 2022), pp. 13245–13255. ISSN: 1463-9084. DOI: 10.1039/D2CP00025C.

[45] D. Frenkel and B. Smit. *Understanding molecular simulation: from algorithms to applications. Vol. 1. Elsevier*. 2001, p. 638. ISBN: 9780080519982.

[46] M. A. Montgomery and M. Elimelech. "Water and sanitation in developing countries: Including health in the equation - Millions suffer from preventable illnesses and die every year". In: *Environmental Science and Technology* 41 (1 Jan. 2007), pp. 17–24. ISSN: 0013936X. DOI: 10.1021/ES072435T.

[47] M. A. Shannon et al. "Science and technology for water purification in the coming decades". In: *Nature* 452 (7185 Mar. 2008), pp. 301–310. ISSN: 14764687. DOI: 10.1038/nature06599.

[48] J. R. Werber, C. O. Osuji, and M. Elimelech. "Materials for next-generation desalination and water purification membranes". In: *Nature Reviews Materials 2016 1:5* 1 (5 Apr. 2016), pp. 1–15. ISSN: 2058-8437. DOI: 10.1038/natrevmats.2016.18.

[49] J. W. Post, H. V. Hamelers, and C. J. Buisman. "Energy Recovery from Controlled Mixing Salt and Fresh Water with a Reverse Electrodialysis System". In: *Environmental Science and Technology* 42 (15 Aug. 2008), pp. 5785–5790. ISSN: 0013936X. DOI: 10.1021/ES8004317.

[50] L. Wen et al. "Construction of biomimetic smart nanochannels with polymer membranes and application in energy conversion systems". In: *Physical Chemistry Chemical Physics* 14 (12 Mar. 2012), pp. 4027–4042. ISSN: 14639076. DOI: 10.1039/C2CP23911F.

[51] Z. Jia et al. "Blue energy: Current technologies for sustainable power generation from water salinity gradient". In: *Renewable and Sustainable Energy Reviews* 31 (Mar. 2014), pp. 91–100. ISSN: 1364-0321. DOI: 10.1016/J.RSER.2013.11.049.

[52] A. Siria, M. L. Bocquet, and L. Bocquet. "New avenues for the large-scale harvesting of blue energy". In: *Nature Reviews Chemistry 2017 1:11* 1 (11 Nov. 2017), pp. 1–10. ISSN: 2397-3358. DOI: 10.1038/S41570-017-0091.

[53] K. S. Novoselov et al. "Electric field in atomically thin carbon films". In: *Science* 306 (5696 Oct. 2004), pp. 666–669. ISSN: 00368075. DOI: 10.1126/SCIENCE.1102896.

[54] A. K. Geim and I. V. Grigorieva. "Van der Waals heterostructures". In: *Nature 2013 499:7459* 499 (7459 July 2013), pp. 419–425. ISSN: 1476-4687. DOI: 10.1038/nature12385.

[55] H. Yoshida et al. "Dripplons as localized and superfast ripples of water confined between graphene sheets". In: *Nature Communications 2018 9:1* 9 (1 Apr. 2018), pp. 1–9. ISSN: 2041-1723. DOI: 10.1038/s41467-018-03829-1.

[56] K. Gopinadhan et al. "Complete steric exclusion of ions and proton transport through confined monolayer water". In: *Science* 363 (6423 Jan. 2019), pp. 145–148. ISSN: 10959203. DOI: 10.1126/SCIENCE.AAU6771.

[57] J. Abraham et al. "Tunable sieving of ions using graphene oxide membranes". In: *Nat. Nanotechnol.* 12 (6 June 2017), pp. 546–550. ISSN: 17483395. DOI: 10.1038/nnano.2017.21.

[58] J. Safaei, P. Xiong, and G. Wang. "Progress and prospects of two-dimensional materials for membrane-based water desalination". In: *Materials Today Advances* 8 (Dec. 2020), p. 100108. ISSN: 2590-0498. DOI: 10.1016/J.MTADV.2020.100108.

[59] S. P. Surwade et al. "Water desalination using nanoporous single-layer graphene". In: *Nature Nanotechnology 2015 10:5* 10 (5 Mar. 2015), pp. 459–464. ISSN: 1748-3395. DOI: 10.1038/nnano.2015.37.

[60] P. Robin, N. Kavokine, and L. Bocquet. "Modeling of emergent memory and voltage spiking in ionic transport through angstrom-scale slits". In: *Science* 373 (6555 Aug. 2021), pp. 687–691. ISSN: 10959203. DOI: 10.1126/SCIENCE.ABF7923.

[61] Y. You et al. "Angstrofluidics: Walking to the Limit". In: *https://doi.org/10.1146/annurev-matsci-081320-032747* 52 (1 July 2022), pp. 189–218. ISSN: 1531-7331. DOI: 10.1146/ANNUREV-MATSCI-081320-032747.

[62] W.-J. Lan et al. "Voltage-Rectified Current and Fluid Flow in Conical Nanopores". In: *Accounts of Chemical Research* 49 (11 2016), pp. 2605–2613. DOI: 10.1021/acs.accounts.6b00395.

[63] T. Zangle, A. Mani, and J. Santiago. "Theory and experiments of concentration polarization and ion focusing at microchannel and nanochannel interfaces". In: *Chemical Society Reviews* 39 (3 2010), pp. 1014–1035. DOI: 10.1039/b902074h.

[64] Y. Zhou and L. Jiang. "Bioinspired Nanoporous Membrane for Salinity Gradient Energy Harvesting". In: *Joule* 4 (11 Nov. 2020), pp. 2244–2248. ISSN: 25424351. DOI: 10.1016/J.JOULE.2020.09.009.

[65] C. Wei, A. J. Bard, and S. W. Feldberg. "Current Rectification at Quartz Nanopipet Electrodes". In: *Analytical Chemistry* 69 (22 Nov. 1997), pp. 4627–4633. ISSN: 00032700. DOI: 10.1021/AC970551G.

[66] Z. Siwy and A. Fuliński. "Fabrication of a Synthetic Nanopore Ion Pump". In: *Physical Review Letters* 89 (19 2002). ISSN: 10797114. DOI: 10.1103/PHYSREVLETT.89.198103.

[67] Z. Siwy et al. "Rectification and voltage gating of ion currents in a nanofabricated pore". In: *Europhysics Letters* 60 (3 Nov. 2002), pp. 349–355. ISSN: 02955075. DOI: 10.1209/EPL/I2002-00271-3.

[68] Z. S. Siwy. "Ion-Current Rectification in Nanopores and Nanotubes with Broken Symmetry". In: *Advanced Functional Materials* 16 (6 Apr. 2006), pp. 735–746. ISSN: 1616-3028. DOI: 10.1002/ADFM.200500471.

[69] L. J. Cheng and L. J. Guo. "Ionic current rectification, breakdown, and switching in heterogeneous oxide nanofluidic devices". In: *ACS Nano* 3 (3 Mar. 2009), pp. 575–584. ISSN: 19360851. DOI: 10.1021/NN8007542.

[70] D. Stein, M. Kruithof, and C. Dekker. "Surface-charge-governed ion transport in nanofluidic channels". In: *Physical Review Letters* 93 (3 July 2004), p. 035901. ISSN: 00319007. DOI: 10.1103/PHYSREVLETT.93.035901.

[71] D. Woermann. "Electrochemical transport properties of a cone-shaped nanopore: high and low electrical conductivity states depending on the sign of an applied electrical potential difference". In: *Physical Chemistry Chemical Physics* 5 (9 Apr. 2003), pp. 1853–1858. ISSN: 1463-9084. DOI: 10.1039/B301021J.

[72] M. Li et al. "Mechanism and performance of ionic diodes fabricated from 2D trapezoidal-shaped nanochannels". In: *Physical Chemistry Chemical Physics* 24 (33 Aug. 2022), pp. 19927–19937. ISSN: 1463-9084. DOI: 10.1039/D2CP03168J.

[73] L. Bocquet and E. Charlaix. "Nanofluidics, from bulk to interfaces". In: *Chemical Society Reviews* 39 (3 Feb. 2010), pp. 1073–1095. ISSN: 1460-4744. DOI: 10.1039/B909366B.

[74] A. K. Geim. "Graphene: Status and prospects". In: *Science* 324 (5934 June 2009), pp. 1530–1534. ISSN: 00368075. DOI: 10.1126/SCIENCE.1158877.

[75] M. Xu et al. "Graphene-like two-dimensional materials". In: *Chemical Reviews* 113 (5 May 2013), pp. 3766–3798. ISSN: 00092665. DOI: 10.1021/CR300263A.

[76] N. Kavokine, M.-L. Bocquet, and L. Bocquet. "Fluctuation-induced quantum friction in nanoscale water flows". In: *Nature 2022 602:7895* 602 (7895 Feb. 2022), pp. 84–90. ISSN: 1476-4687. DOI: 10.1038/S41586-021-04284-7.

[77] A. Keerthi et al. "Ballistic molecular transport through two-dimensional channels". In: *Nature 2018 558:7710* 558 (7710 June 2018), pp. 420–424. ISSN: 1476-4687. DOI: 10.1038/S41586-018-0203-2.

[78] A. K. Geim. "Exploring Two-Dimensional Empty Space". In: *Nano Letters* 21 (15 Aug. 2021), pp. 6356–6358. ISSN: 15306992. DOI: 10.1021/ACS.NANOLETT.1C02591.

[79] S. J. Haigh et al. "Cross-sectional imaging of individual layers and buried interfaces of graphene-based heterostructures and superlattices". In: *Nature Materials 2012 11:9* 11 (9 July 2012), pp. 764–767. ISSN: 1476-4660. DOI: 10.1038/nmat3386.

[80] P. Loche et al. "Breakdown of Linear Dielectric Theory for the Interaction between Hydrated Ions and Graphene". In: *Journal of Physical Chemistry Letters* 9 (22 Nov. 2018), pp. 6463–6468. ISSN: 19487185. DOI: 10.1021/ACS.JPCLETT.8B02473.

[81] H. Zhu et al. "Investigation of dielectric constants of water in a nano-confined pore". In: *RSC Advances* 10 (15 Feb. 2020), pp. 8628–8635. ISSN: 2046-2069. DOI: 10.1039/C9RA09399K.

[82] C. Qi et al. "Anomalously Low Dielectric Constant of Ordered Interfacial Water". In: *Journal of Physical Chemistry Letters* 12 (2 Jan. 2021), pp. 931–937. ISSN: 19487185. DOI: 10.1021/ACS.JPCLETT.0C03299.

[83] S. Mondal and B. Bagchi. "Water Layer at Hydrophobic Surface: Electrically Dead but Dynamically Alive?" In: *Nano Letters* 20 (12 Dec. 2020), pp. 8959–8964. ISSN: 15306992. DOI: 10.1021/ACS.NANOLETT.0C04312.

[84] Y. Zhang et al. "Water dynamics at electrified graphene interfaces: a jump model perspective". In: *Physical Chemistry Chemical Physics* 22 (19 May 2020), pp. 10581–10591. ISSN: 1463-9084. DOI: 10.1039/D0CP00359J.

[85] J. F. Olivieri, J. T. Hynes, and D. Laage. "Confined water's dielectric constant reduction is due to the surrounding low dielectric media and not to interfacial molecular ordering". In: *Journal of Physical Chemistry Letters* 12 (17 May 2021), pp. 4319–4326. ISSN: 19487185. DOI: 10.1021/ACS.JPCLETT.1C00447.

[86] L. O. Chua. "Memristor—The Missing Circuit Element". In: *IEEE Transactions on Circuit Theory* 18 (5 1971), pp. 507–519. ISSN: 00189324. DOI: 10.1109/TCT.1971.1083337.

[87] L. Chua. "If it's pinched it's a memristor". In: *Semiconductor Science and Technology* 29 (10 Sept. 2014), p. 104001. ISSN: 0268-1242. DOI: 10.1088/0268-1242/29/10/104001.

[88] D. B. Strukov et al. "The missing memristor found". In: *Nature 2008 453:7191* 453 (7191 May 2008), pp. 80–83. ISSN: 1476-4687. DOI: 10.1038/NATURE06932.

[89] A. L. Hodgkin, A. F. Huxley, and B. Katz. "Measurement of current-voltage relations in the membrane of the giant axon of Loligo". In: *The Journal of Physiology* 116 (4 Apr. 1952), p. 424. ISSN: 14697793. DOI: 10.1113/JPHYSIOL.1952.SP004716.

[90] *Insane in the Chromatophores - YouTube*. URL: https://www.youtube.com/watch?v=G-OVrI9x8Zs.

[91] Y. Hou and X. Hou. "Bioinspired nanofluidic iontronics". In: *Science* 373 (6555 Aug. 2021), pp. 628–629. ISSN: 10959203. DOI: 10.1126/SCIENCE.ABJ0437.

[92] P. Robin et al. "Long-term memory and synapse-like dynamics of ionic carriers in two-dimensional nanofluidic channels". In: (May 2022). DOI: 10.48550/arxiv.2205.07653.

[93] K. J. Tielrooij et al. "Anisotropic water reorientation around ions". In: *Journal of Physical Chemistry B* 115 (43 Nov. 2011), pp. 12638–12647. ISSN: 15205207. DOI: 10.1021/JP206320F.

[94] L. X. Dang et al. "Ion Solvation in Polarizable Water: Molecular Dynamics Simulations". In: *Journal of the American Chemical Society* 113 (7 1991), pp. 2481–2486. ISSN: 15205126. DOI: 10.1021/JA00007A021.

[95] S. Sahu and M. Zwolak. "Ionic selectivity and filtration from fragmented dehydration in multilayer graphene nanopores". In: *Nanoscale* 9 (32 Aug. 2017), pp. 11424–11428. ISSN: 2040-3372. DOI: 10.1039/C7NR03838K.

[96] M. Xue et al. "Ion Hydration under Nanoscale Confinement: Dimensionality and Scale Effects". In: *Journal of Physical Chemistry Letters* 13 (2022), pp. 4815–4822. ISSN: 19487185. DOI: 10.1021/ACS.JPCLETT.2C00817.

[97] R. Zangi and J. B. Engberts. "Physisorption of hydroxide ions from aqueous solution to a hydrophobic surface". In: *Journal of the American Chemical Society* 127 (7 Feb. 2005), pp. 2272–2276. ISSN: 00027863. DOI: 10.1021/JA044426F.

[98] R. Eisenschitz and F. London. "Über das Verhältnis der van der Waalsschen Kräfte zu den homöopolaren Bindungskräften". In: *Zeitschrift für Physik 1930 60:7* 60 (7 July 1930), pp. 491–527. ISSN: 14346001. DOI: 10.1007/BF01341258.

[99] A. P. Thompson et al. "LAMMPS - a flexible simulation tool for particle-based materials modeling at the atomic, meso, and continuum scales". In: *Computer Physics Communications* 271 (Feb. 2022), p. 108171. ISSN: 0010-4655. DOI: 10.1016/J.CPC.2021.108171.

[100] W. Humphrey, A. Dalke, and K. Schulten. "VMD: Visual molecular dynamics". In: *Journal of Molecular Graphics* 14 (1 Feb. 1996), pp. 33–38. ISSN: 0263-7855. DOI: 10.1016/0263-7855(96)00018-5.

[101] H. J. Berendsen, J. R. Grigera, and T. P. Straatsma. "The missing term in effective pair potentials". In: *Journal of Physical Chemistry* 91 (24 2002), pp. 6269–6271. ISSN: 00223654. DOI: 10.1021/J100308A038.

[102] Y. Zhao et al. "Coupled Transport of Water and Ions through Graphene Nanochannels". In: *Journal of Physical Chemistry C* 124 (31 Aug. 2020), pp. 17320–17330. ISSN: 19327455. DOI: 10.1021/ACS.JPCC.0C04158.

[103] S. Salman et al. "Effect of temperature on the coupling transport of water and ions through a carbon nanotube in an electric field". In: *Journal of Chemical Physics* 153 (18 Nov. 2020), p. 184503. ISSN: 10897690. DOI: 10.1063/5.0028077.

[104] H. W. Horn et al. "Development of an improved four-site water model for biomolecular simulations: TIP4P-Ew". In: *The Journal of Chemical Physics* 120 (20 May 2004), p. 9665. ISSN: 0021-9606. DOI: 10.1063/1.1683075.

[105] G. Ciccotti and J. P. Ryckaert. "Molecular dynamics simulation of rigid molecules". In: *Computer Physics Reports* 4 (6 Sept. 1986), pp. 346–392. ISSN: 0167-7977. DOI: 10.1016/0167-7977(86)90022-5.

[106] H. D. Whitley and D. E. Smith. "Free energy, energy, and entropy of swelling in Cs–, Na–, and Sr–montmorillonite clays". In: *The Journal of Chemical Physics* 120 (11 Mar. 2004), p. 5387. ISSN: 0021-9606. DOI: 10.1063/1.1648013.

[107] G. Giunta. *Personal communication*. 2022.

[108] W. R. Cannon, B. M. Pettitt, and J. A. McCammon. "Sulfate Anion in Water: Model Structural, Thermodynamic, and Dynamic Properties". In: *Journal of Physical Chemistry* 98 (24 2002), pp. 6225–6230. ISSN: 00223654. DOI: 10.1021/J100075A027.

[109] T. Mouterde et al. "Molecular streaming and its voltage control in ångström-scale channels". In: *Nature 2019 567:7746* 567 (7746 Mar. 2019), pp. 87–90. ISSN: 1476-4687. DOI: 10.1038/S41586-019-0961-5.

[110] Z.-Q. Wu et al. "Synergistic Effect of Electrostatic Interaction and Ionic Dehydration on Asymmetric Ion Transport in Nanochannel/Ion Channel Composite Membrane". In: *The Journal of Physical Chemistry Letters* 13 (June 2022), pp. 5267–5274. ISSN: 1948-7185. DOI: 10.1021/ACS.JPCLETT.2C01166.

[111] D. Trzesniak, A. P. E. Kunz, and W. F. V. Gunsteren. "A Comparison of Methods to Compute the Potential of Mean Force". In: *ChemPhysChem* 8 (1 Jan. 2007), pp. 162–169. ISSN: 1439-7641. DOI: 10.1002/CPHC.200600527.

[112] S. Bielfeldt. "Dissolved Ionic Salts under Nanoconfinement". Institute for Theoretical Physics, July 2022.

[113] D. J. Griffiths. "Introduction to Electrodynamics". In: *Introduction to Electrodynamics* (June 2017). DOI: 10.1017/9781108333511.

[114] J. K. Gregory et al. "The Water Dipole Moment in Water Clusters". In: *Science (New York, N.Y.)* 275 (5301 Feb. 1997), pp. 814–817. ISSN: 1095-9203. DOI: 10.1126/SCIENCE.275.5301.814.

[115] Z. Wan et al. "Anomalous water transport in narrow-diameter carbon nanotubes". In: *Proceedings of the National Academy of Sciences of the United States of America* 119 (39 Sept. 2022). ISSN: 10916490. DOI: 10.1073/PNAS.2211348119.

[116] J. Su and D. Huang. "Coupling Transport of Water and Ions Through a Carbon Nanotube: The Role of Ionic Condition". In: *Journal of Physical Chemistry C* 120 (20 May 2016), pp. 11245–11252. ISSN: 19327455. DOI: 10.1021/ACS.JPCC.6B01851.

A Lennard-Jones Parameters

As explained in the Methods section, we used Lennard-Jones potentials for the atoms and the walls. We used the same parameters for the ions as Ref. [60], and used the SPC/E model for water atoms [101]. The parameters that were used are all shown in Table 1.

	ε (kcal/mol)	σ (Å)	q/e	m (g/mol)
O (H_2O)	0.1553	3.166	– 0.8476	15.9994
H	0	1	+ 0.4238	1.008
Na	0.123	2.35	+ 1	28.990
Cl	0.1	4.401	– 1	35.453
S	0.25	3.55	+ 2	32.065
O (SO_4)	0.1553	3.166	– 1	15.9994
Ca	0.1	2.895	+ 2	40.078
X	0.1	2.895	+ 2	40.078
Y	0.1	2.895	– 2	40.078
LJ 9-3 wall	0.478	3.214	0	∞

Table 1: Lennard-Jones parameters, charge and mass of all the used atoms.

The effective ε for the Lennard-Jones 9-3 wall, is calculated with

$$\varepsilon_{eff} = \frac{2\pi}{3}\rho_C\sigma_C^3\varepsilon_C \tag{A.1}$$

where the average carbon density in graphite is $\rho_C = 0.121$ Å^{-3} is calculated using the interlayer distance and the bond length of graphite [75]. The other parameters of carbon are also taken from Robin *et al.* [60]: $\sigma_C = 3.214$ Å and $\varepsilon_C = 0.0566$ kcal/mol. The mass of the wall is assumed to be infinite.

We also simulate two covalently bonded molecules: water (H_2O) and sulfate (SO_4). The water molecules are kept rigid with the SHAKE algorithm, while the sulfate molecules are kept rigid with LAMMPS 'rigid' command because SHAKE cannot handle molecules that consist of five atoms. Both molecules have tetrahedral internal angles of $\theta = 109.47^o$. Water has a bond length of $r_{OH} = 0.96$ Å, and sulfate has $r_{SO} = 1.49$ Å.

B Straight Channels

In the main text, we mostly focus on the dynamics of ions and water in tapered channels. We present phenomena there, which we argue are due to the divergence of the polarization in the channel, which is in turn caused by the asymmetry in the geometry. That begs the question, of course, about whether they are then absent in the case where the side walls are straight, or where there are no side walls at all. This turns out to be the case, and we will discuss some of the results in these straight channels, to function as a control group of sorts.

In Section 4.4, we observed a remarkably strong asymmetry in the ionic fluxes. The ion moving in the positive y direction was almost the sole contributor to the current. This is in sharp contrast to the behaviour that is expected without any tapered geometry. We expect that the mobility ratio between the cation and anion is constant and independent on the value or direction of the electric field. The current contributions of NaCl in a regular geometry, without any side walls, is shown in Fig. 41a. We see that, indeed, the contributions of sodium and chloride are roughly equal. We also look at the case where there are side walls, but they are straight, meaning $\xi = 1$. This is shown in Fig. 41b, and we see that there also, the slopes of the current contribution do not depend much on the sign and value of the electric field. The uncertainty in this case is very big because all the ions have to move through a relatively small region, but we do not see the unidirectional fluxes that we observe for $\xi < 1$.

We also look at the average water flow of channels without these tapered walls. If our hypothesis is correct, the average water velocity should vanish in these systems. In Fig. 42a we plot the average water velocity for the regular geometry in which there are no side walls. We see that indeed there is

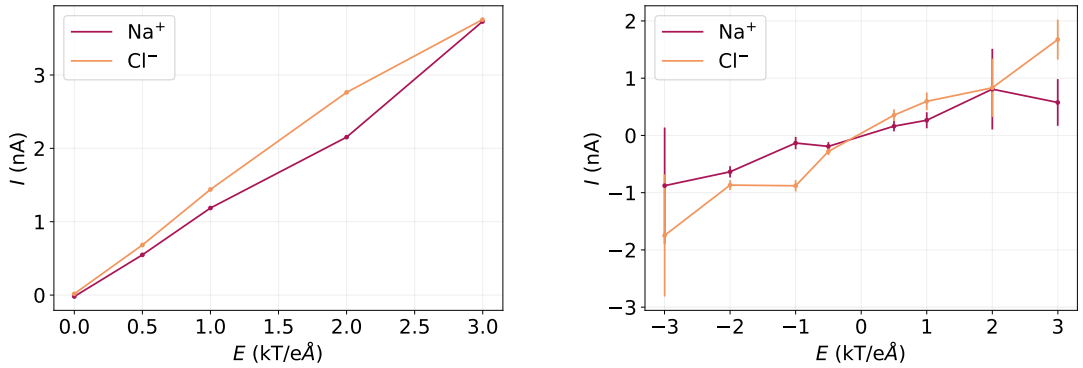

(a) (b)

Figure 41: Current contributions of NaCl as a function of the external electric field in systems that do not exhibit an asymmetry. (a) Current contributions in a regular geometry without side walls. (b) Current contributions in system with $D_m = 60$ Å and $\xi = 1$.

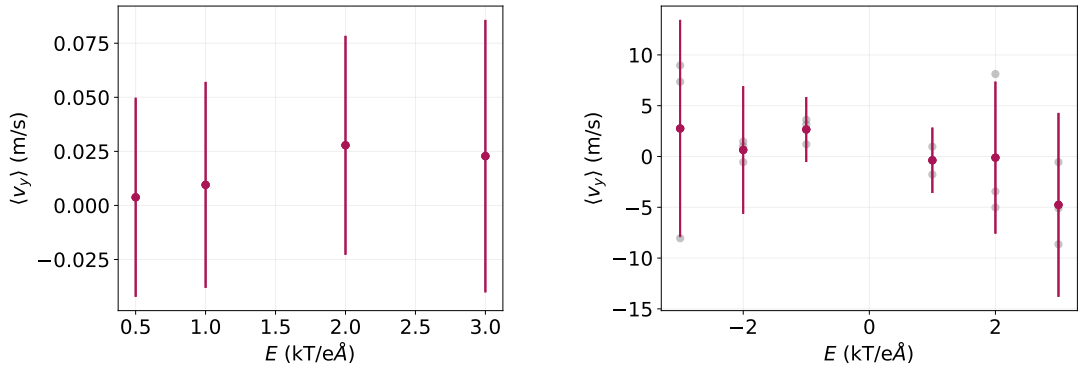

(a) (b)

Figure 42: Average water velocity through straight channels. (a) Regular geometry without side walls. (b) System with $\xi = 1$ and $D_m = 60$ Å. The average velocities of individual runs are shown in grey.

barely any water flow. The flow is less than 1% of that found in Section 4.8. The case where there are straight side walls is shown in Fig. 42b. Here the magnitude of the average velocites is similar to those of $\xi < 1$ for some electric fields, while it is around 0 for others. We also note that the sign of the water flow can differ in individual simulations with this geometry. For $E = -3$, -2, 1 and 2 kT/eÅ, for instance, we see that the individual water velocities are distributed around zero, which was never the case for any other geometries. It seems that the average velocity oscillates around 0, but has a high variability. If there is any trend in this data at all, it would have a downwards slope, more akin to the water fluxes observed in nanotubes in Ref. [116]. However, this effect seems to be much smaller than the flow that we observed in Section 4.

C Layman's summary

Okay, so after scrolling through this thesis, you may be wondering 'what is this thesis really about? And now without all the jargon please.' Let me quickly go over the question we try to answer here, without assuming a master degree in physics this time (or any STEM field at all, for that matter). It's about salt water. In essence, we are talking about how water and salt behave when you squeeze them between two sheets of a material called graphene. And we're doing this on an incredibly small scale! The distance between the sheets is only one nanometer, which is one billionth of a meter, or 0.001% of the width of a single hair. The space between them that contains the water and salt is what we call a nanoslit. Now this begs the question of course, why would you ever want to do this? Why do we care about water and salt that we squished until they formed a layer of only a single nanometer thick? It seems weirdly specific and horribly impractical.

Well, it turns out that water and salt are very weird in this environment, and in science weird things kind of make it all interesting. Salt usually dissolves when you put it in water. It does something different, however, when it's in a really small space. Suddenly salt can start to form these crystal grains up again [31], even when in water. That is only just one part of the weird behaviour of water and salt at this scale, and it has some really cool applications! Some researchers from Paris used it to mimic brain cells, for instance [60]. They did this by combining several of these nanoslits in a clever way, and creating ion currents through them in a specific way.

When you think of electric current, you're probably thinking about the currents that come out of power sockets or from a battery. These are currents that are caused by electrons that move through wires. These electrons have an electrical charge that can move, and that specifically is what we call a current. Now similarly, you can have a current of ions through water. Ions are charged atoms that make up salt. Table salt is NaCl, for instance, which is a positively charged sodium (Na^+) ion and a negatively charged chloride (Cl^-) atom. This means that you can also get a current by connecting salt water to a battery. This battery generates an electrical field which makes positive ions move towards the negative pole of the battery and the negative ions move towards the positive pole. With these ion currents in nanoslits and nanochannels, you can do all sorts of things. I already mentioned the (simple) artificial brain cell that made use of the nanoslits [60], but you can also generate power with nanochannels [50–52], or desalinate water [48, 49]. For some of these applications however, it is important that the ion currents are partially blocked in one direction, but are free to move in the other. That is what we are after. We want to find a way to make the ion currents in nanoslits asymmetric with respect to the direction of the electric field.

We look for this using computer simulations. Making these systems in the laboratory is very hard, and having two left hands made me quickly realize in university that experimental work was not for

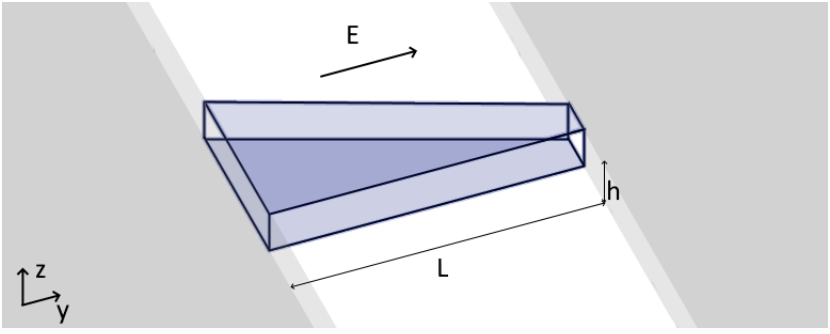

Figure 43: Sketch of the system that we look into.

me. Moreover, there is only a handful of people in the world who can actually make these things, of which about 20 % won a Nobel prize [53], so I don't feel too bad about it. Anyway, we simulate all kinds of nanoslits with different strengths and directions of the electric field, and see if we can spot any asymmetries. And we did! It turns out that there is a small asymmetry when you put some side walls into your system under an angle. I made a quick sketch of the system, which is shown above. Now of course, we also want to know what causes this asymmetry. In principle, there is no known reason in literature why there would be this asymmetry so this is a very interesting question.

We actually notice another very weird thing when we look at how the individual ions move. It turns out that ions only want to move from the wide side to the small side, but not the other way around. You would expect that both happen equally often, because positive ions want to move in the direction of the electric field and negative ions want to move the other way. But only the ion that wants to move 'upwards' is let through, so these nanoslits filter the water! This is often called 'ion selectivity' in the literature. It is really unexpected and interesting that this happens in this system, so we want to find out why this happens.

We quickly identify water as a suspect for the filtering effect.[5] I already mentioned that positive ions want to move one way and negative ions the other way, when you apply an electric field (with a battery for instance). This is more general, however, and actually all positive and negative charges want to move in opposite ways in an electric field. It just so happens that water molecules have both a positive and a negative side; the oxygen atom (O) is slightly negative, and the two hydrogen atoms (H) are slightly positive. This means that the oxygen atom wants to move to the positive pole of the battery, and the hydrogen wants to move to the negative pole. They are stuck together, however, and so they cannot really move either way, but they will reorient themselves such that the negative oxygen is closest to the positive pole, and the hydrogen atoms are closest to the negative pole. This is what we call polarization; all the water molecules point roughly in the same direction when there is an electric field.

When the molecules all point in exactly the same direction, nothing interesting would happen. However, because of the shape and size of the channel and the material of the wall, the polarization isn't neatly as strong and in the same direction everywhere. Near the tip of the channel it is much stronger than elsewhere in the system. When there are more water molecules pointing towards some point in the channel than point away from the channel, you get a charged region. We call this a 'bound charge'. A sketch of a situation where that happens very extremely is shown below in Fig. 44(a). Here the water molecules are sketched as just a positive and negative blob together, but the '+' stand for two hydrogen atoms, and the '-' for the oxygen atom. In our system, the water does not point this extremely towards one point, but there are regions that have on average a bound charge.

In our system, we notice a bound charge near the narrow end of the channel. This bound charge is negative for positive electric fields, and negative for positive electric fields. These charges influence the ions; negative bound charge repels negative ions, and similarly, positive bound charge repel positive ions. This means that there is a small barrier for the ions to go into the tip. A (slightly exaggerated) sketch of what happens is shown in Fig. 44(b). In principle, this could explain what we saw, namely, ions moving only from the wide end to the small end, but not the other way around. We did some tests, however, and it turns out that this bound charge is not strong enough to keep all the ions from moving downwards through the channel. It probably reduces the number of ions that move downwards a bit, but it cannot possibly stop all of them. So it turns out, we need something else to explain this.

[5] And by 'quickly' I mean that it is the first thing we show in this thesis. In real time, it took a solid 6 months or so.

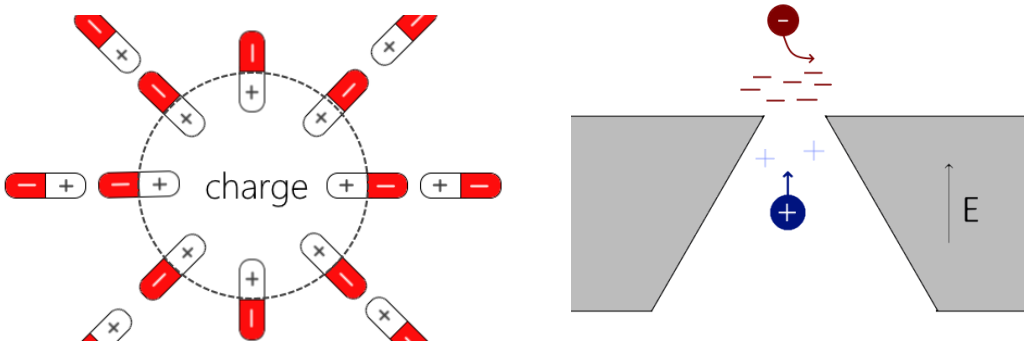

(a) (b)

Figure 44: (a) Sketch of a so-called divergence of the polarization. Here there is a region in the middle where there are more molecules pointing inwards than outwards. This causes a bound charge. (b) Sketch of what happens due to the divergence in the polarization of water.

The missing piece of the puzzle turns out to be the flow of water in the system. The divergence of the polarization introduces a small asymmetry in the ion fluxes, so more ions move upwards than downwards. These ions drag water with them, however, and therefore set the water in motion. As a consequence, it gets harder for ions to move against the fluid flow, while it gets easier to move in the same direction of the water. This means that the flux of the ion species moving upwards through the channel increases, while the flux of the ions species that moves downwards through the channel decreases. This explains the ion fluxes that only move in one direction!

To conclude, we looked at the ion fluxes through a tapered nanoslit and observed an interesting ion selectivity; one ion species is moving through the channel, but the other one is not. We show that this is because of the interaction of the ion with the divergence in the polarization of the water. This causes an initial asymmetry in the fluxes – so slightly more ions move upwards through the channel than downwards. This in turn causes the water to flow very rapidly, which helps the ions that move in the same direction as the fluid flow, and hinders the ion that is moving against the flow. This is a new mechanism that has not been described before in literature, and that could potentially be used to mimic biological channels.

D Acknowledgements

It has been an absolute pleasure to work on this thesis for the past year. I would like to thank my supervisors Marjolein Dijkstra and René van Roij. I am extremely grateful for their great support and feedback during this project. Secondly, I would like to thank them for introducing me to the field. It was the courses that they taught in the bachelor and master and their enthusiasm that got me excited for soft matter physics. I am very excited to continue working in this field and to keep learning. I also want to thank my daily supervisors Gerardo Campos-Villalobos and Giuliana Giunta for all their help and support. I am very grateful for their guidance and endless patience in helping me with the LAMMPS codes. I also want to thank Sebastian Bielfeldt, Floris van den Bosch and Thijs ter Rele for the many interesting conversations about the subject.

I would also like to thank Thijs ter Rele for printing my thesis for me a few times, saving me a few euros. He jokingly asked me today to formally thank him for this in my thesis, and should have known that I would actually do it. Many thanks also to the study group that got me through the first semester of this master. Those late-night group calls working on the latest Quantum Field Theory or General Relativity hand-ins in the middle of the covid lockdowns are the only reason I passed. Special thanks to all my fellow students and my friends and family for helping and supporting me through my studies. Specifically, I am very grateful to my good friend Cintia Perugachi-Israels for all the fun work sessions and for proof reading the first few drafts of this thesis, which resulted in a thesis that is significantly less horrible to read than the first draft.